Demographic basis of spatially structured fluctuations in a threespine stickleback metapopulation

Joseph S. Phillips[1,2,†,‡,ORCID]

Árni Einarsson[3,4]

Kasha Strickland[1,§,ORCID]

Anthony R. Ives[2,ORCID]

Bjarni K. Kristjánsson[1,ORCID]

Katja Räsänen[5,6,ORCID]

1. Department of Aquaculture and Fish Biology, Hólar University, Sauðárkrókur 551 Iceland

2. Department of Integrative Biology, University of Wisconsin-Madison, Madison, Wisconsin 53706 USA

3. Mývatn Research Station, IS-660 Mývatn, Iceland

4. Faculty of Life and Environmental Sciences, University of Iceland, 101 Reykjavík, Iceland

5. Department of Aquatic Ecology, EAWAG and Institute of Integrative Biology, ETH Zurich, Überlandstrasse 133, CH-8600 Dübendorf, Switzerland

6. Department of Biological and Environmental Sciences, University of Jyväskylä, 40014, Jyväskylä, Finland

† Present address: Department of Biology, Creighton University, Omaha, Nebraska 68178 USA

‡ E-mail: josephphillips@creighton.edu

§ Present address: School of Biological Sciences, University of Edinburgh, Edinburgh, UK EH8 9JX

Keywords: demographic transience, *Gasterosteus aculeatus*, Mývatn, population cycles, spatial synchrony, state-space model

Manuscript type: E-Article.

Prepared using the suggested LaTeX template for *Am. Nat.*

Abstract

Uncovering the demographic basis of population fluctuations is a central goal of population biology. This is particularly challenging for spatially structured populations, which require disentangling synchrony in demographic rates from coupling via movement between locations. In this study, we fit a stage-structured metapopulation model to a 29-year times series of threespine stickleback abundance in the heterogeneous and productive Lake Mývatn, Iceland. The lake comprises two basins (North and South) connected by a channel through which the stickleback disperse. The model includes time-varying demographic rates, allowing us to assess the potential contributions of recruitment and survival, spatial coupling via movement, and demographic transience to the population's large fluctuations in abundance. Our analyses indicate that recruitment was only modestly synchronized between the two basins, whereas survival probabilities of adults were more strongly synchronized, contributing to cyclic fluctuations in the lake-wide population size with a period of approximately six years. The analyses further show that the two basins were coupled through movement, with the North Basin subsidizing the South Basin and playing a dominant role in driving the lake-wide dynamics. Our results show that cyclic fluctuations of a metapopulation can be explained in terms of the combined effects of synchronized demographic rates and spatial coupling.

Introduction

Temporal fluctuations in demographic processes such as survival and reproduction are of central importance to population biology (Twombly, 1994; Fox and Gurevitch, 2000; Koons et al., 2016). Changes in demographic rates underpin population fluctuations (Coulson et al., 2005), and these changes can arise from both endogenous processes such as predator-prey interactions (Rosenzweig and MacArthur, 1963) and exogenous processes such as climatic variability (Elton, 1924). Furthermore, demographic rates can change in response to trait plasticity and evolution (Ellner et al., 2011; Bonnet et al., 2019), and the interplay between ecological and evolutionary dynamics in wild populations is often predicated on the potential for demographic rates to vary through time (Coulson et al., 2006; Siepielski et al., 2009; Ozgul et al., 2010; Ellner et al., 2011). While temporal variation in demographic rates has been extensively studied, these studies are often restricted to populations subject to long-term monitoring with repeated observations of uniquely identified individuals (e.g., mark-recapture; Fujiwara and Caswell, 2002), which may not be representative of the full range of dynamics found in wild populations. Furthermore, long-term demographic studies often focus on directional trends or responses to specific drivers such as predator removal (e.g., Diller et al., 2016) or climate change (Hunter et al., 2010), rather than addressing population fluctuations per se (but see White et al., 2007; Koons et al., 2017; Taylor et al., 2018; Hoy et al., 2020). Consequently, there is a need for further studies characterizing the demographic underpinnings of population fluctuations, especially in systems that are generally underrepresented in long-term demographic studies.

Uncovering the demographic basis of population fluctuations can be particularly challenging for metapopulations (Bjørnstad et al., 1999), in which discrete patches or sub-populations are linked through movement (i.e., immigration and emigration) (Hanski, 1998). Synchronous fluctuations in patch-level abundance will tend to reinforce each other in the metapopulation dynamics, while asynchronous or compensatory fluctuations will tend to cancel each other out (Liebhold et al., 2004). The degree of synchrony between the patch-level dynamics will be influenced by

the extent to which the within-patch demographic rates (e.g., reproduction and survival) are synchronized between patches (Ranta et al., 1995; Liebhold et al., 2004). Synchronization could arise from synchronous changes in environmental drivers such as climate (Moran, 1953) or through patches being indirectly coupled by joint interactions with another dynamic agent such as a mobile predator (Ims and Andreassen, 2000; Gilg et al., 2009). Moreover, direct coupling between patches via movement can alter the patch-level dynamics (Liebhold et al., 2004), and the effect of movement on the metapopulation dynamics interacts with processes occurring within patches (Ranta et al., 1995; Kendall et al., 2000; Goldwyn and Hastings, 2008). Disentangling the effects of direct coupling through movement, the degree of synchrony between demographic processes within patches, and the interplay between the two is an important step in characterizing metapopulation fluctuations (Liebhold et al., 2004; Abbott, 2011).

Further complicating efforts to characterize the demographic basis of population fluctuations is the potential role of transience. "Transience" refers to short-term dynamics of a system that differ from the long-term or asymptotic dynamics under a fixed set of conditions (Hastings, 2010). A fixed set of demographic rates for a demographically structured population implies an equilibrium distribution of individuals across population states such as stage classes or patches (Caswell, 2001). After an external perturbation, the population's state distribution will tend towards its equilibrium, and this will generally entail transient changes in the total population growth rate. The qualitative behavior of demographic transience depends on the exact configuration of demographic rates but can include cyclic fluctuations as the population approaches its equilibrium distribution (Caswell, 2001). By definition, these transient fluctuations can occur without temporal variation in the underlying per capita demographic rates. Rather, transient fluctuations arise because of changes in the distribution of individuals across demographic states, which scales the relative contributions of the per capita rates to the overall population growth rate. When per capita demographic rates vary through time, which is true to at least some extent for all wild populations, the equilibrium distribution will be a "moving target" such that a given population is likely to be in a perpetual state of disequilibrium (Fox and Gurevitch, 2000; Koons

et al., 2017). Whether such perpetual disequilibrium results in large transience depends on the extent to which the underlying demographic rates change through time and the rate at which the population approaches its ever-changing equilibrium distribution, which is itself a function of the time-specific demographic rates (Caswell and Neubert, 2005; Caswell, 2007). Despite growing recognition (Caswell, 2007; Koons et al., 2017), the contribution of transience to fluctuations in wild populations is generally unknown (but see Hoy et al., 2020).

In this study, we analyzed the metapopulation fluctuations of threespine stickleback (*Gasterosteus aculeatus*) over the course of three decades in Lake Mývatn, Iceland. The Mývatn stickleback population is spatially structured by the geomorphology of the lake (Gíslason et al., 1998; Millet et al., 2013), which is divided into two basins connected by two narrow channels (Figure 1 A). The larger South Basin (Syðriflói; 28 km^2) is dominated by exposed sediment and intermittent mats of filamentous green algae (Einarsson et al., 2004). The substantially smaller North Basin (Ytriflói; 8.5 km^2) is more spatially heterogeneous, in part due to dredging of the lake bottom that substantially altered its bathymetry. The North Basin has historically sustained much higher densities of threespine stickleback than the South Basin (Gíslason et al., 1998), presumably due to the ecological differences between the basins. Despite the narrow connection between the basins, population genetic analyses indicate limited differentiation (Millet et al., 2013), which implies extensive gene flow and admixture. This is consistent with previous studies indicating that lacustrine populations of threespine sticklebacks have the potential to be well-mixed through extensive within-lake dispersal (Maciejewski et al., 2020).

In addition to its spatial heterogeneity, the Mývatn stickleback population fluctuates substantially through time. While the causes of these fluctuations are unknown, they are likely connected to the large temporal variability of other species in the lake. Mývatn is naturally eutrophic due to inflows of nutrient-rich springs, which sets the stage for high-amplitude fluctuations in secondary producers (Einarsson et al., 2004). Chief among these are various species of rotifers, chironomids, and crustaceans (Einarsson et al., 2002; Einarsson and Örnólfsdóttir, 2004; Garðarsson et al., 2004; Ives et al., 2008), some of which are important food sources for threespine

stickleback (Guðmundsson, 1996). Moreover, the lake hosts temporally variable populations of Arctic charr (*Salvelinus alpinus*), brown trout (*Salmo trutta*), and piscivorous birds that have the potential to induce fluctuations in the stickleback population from the top down (Garðarsson, 1979; Guðbergsson, 2004; Phillips et al., 2022). Finally, Mývatn's stickleback can sustain high loads of the tapeworm *Schistocephalus solidus* (Gíslason et al., 1998; Karvonen et al., 2013), which substantially reduces fecundity in other threespine stickleback populations (Heins et al., 2010; Heins, 2012).

To characterize the spatiotemporal dynamics of the Mývatn stickleback population, we fit a stage-structured metapopulation model (Caswell, 2001) to a 29-year time series of stickleback abundance. The model includes temporal variation in basin-level recruitment and survival, as well as movement between basins. Changes in these demographic rates were statistically inferred as required to fit the observed population dynamics. This approach provides great flexibility in modeling the demographic underpinnings of population fluctuations, including those implicitly arising from exogenous and endogenous processes (Zeng et al., 1998; Ives and Dakos, 2012; Phillips et al., 2022). Equipped with the parameterized model, we quantified the synchrony in recruitment and survival between the two basins in addition to the degree of coupling through movement. Furthermore, we estimated both the direct (i.e., asymptotic) and indirect (i.e., transient) effects of time-varying recruitment, survival, and movement on the metapopulation dynamics. Our analysis illustrates how spatially structured fluctuations can arise through the conjunction of spatial synchrony in demographic rates and spatial coupling through movement in a wild population.

Methods

Long-term data collection

From 1991 to 2020, the stickleback population of Mývatn was surveyed in June and August of each year (hereinafter "June census" and "August census", respectively). These surveys were

conducted under the auspices of the Mývatn Research Station, which has government approval for collecting fish specimens from the lake (animal ethics review is not legally required in Iceland for wild-caught fish euthanized upon capture). We sampled eight off-shore sites, five in the South Basin and three in the North Basin (Figure 1 A). These sites provided wide coverage of the lake, with the exception of the eastern portion of the South Basin that has historically had negligible densities of sticklebacks. The sites exhibited different substrates, with two broad categories being bare sediment (possibly with some cover by filamentous green algae) and sediment covered with various species of vascular macrophyte; both categories have representative sites in each basin (see detailed site descriptions in Millet et al., 2013).

For each site and survey event, we set unbaited minnow traps (c. 3.2 mm mesh size) for two 12-hour sessions, one during the day and one during the night. Typically, five traps were set and counted separately, although occasionally fewer traps were set, or trap-catches were pooled for a given site prior to counting. Trapped individuals were sorted into two size-classes (small and large) with a threshold of 50 mm in June and 45 mm in July (Gíslason et al., 1998). Although there is likely variation in size at maturation (Singkam and MacColl, 2019), these size classes are expected to generally correspond with sexual maturity (Guðmundsson, 1996; Gíslason et al., 1998), and for the purposes of demographic modeling (described below) we interpreted them as two stage-classes: juvenile (small) and adult (large). In general, threespine stickleback reach maturity at 1-2 years of age (Baker et al., 2008), although age and size at maturation are plastic traits (Baker et al., 2015) that may differ among populations (Snyder, 1991).

We used site-level catch per unit effort (CPUE) for each of the two stage-classes at each time point to parameterize the metapopulation model described below. CPUE was calculated for each site and sampling event by summing across all traps set during both day and night sampling and then dividing by the total number of traps. Within each basin and stage class, site-level catches were of comparable magnitude and generally correlated through time (Figure 1 B). Therefore, while we used site-level CPUE to parameterize the model, the model itself was formulated in terms of relative basin-level abundance, with the sites serving as repeated observations of the

same basin-level abundance estimate, as described in more detail below.

We grouped site 135 with the rest of the South Basin (Figure 1 A), despite its location on the boundary between the two basins, as its stickleback catch was similar to other sites within the South Basin in most years. However, we acknowledge that an unusually large number of adults were trapped at site 135 in 2019 and 2020, which may not be fully captured in our basin-level analysis. Moreover, we acknowledge the inherent uncertainties in catch data for fish populations, and in particular the possibility that the catch probability varied among sites due to local conditions such as substrate. However, our model was formulated in terms of basin-level abundance (with each basin encompassing a range of substrates), and the higher densities in the North Basin implied by the trapping data are consistent with a previous mark-recapture study (Gíslason et al., 1998). Furthermore, the data were collected with a consistent methodology and equipment by the same researchers for the duration, which should improve the credibility of the inferred temporal patterns that are the major focus of our analysis.

Metapopulation model

We used a stage-structured metapopulation model (Caswell, 2001) with time-varying demographic rates to characterize the dynamics of the stickleback population. The model projected the population dynamics due to recruitment, survival, and stage transitions from juvenile to adult within each basin, as well as movement between basins. Recruitment, survival, and movement were allowed to vary through time, enabling the model to characterize a range of dynamics, including those implicitly due to endogenous (e.g., density dependence) and exogenous (e.g., environmental variation) processes (Zeng et al., 1998; Ives and Dakos, 2012; Phillips et al., 2022). We estimated the demographic rates by fitting the model to the time series of CPUE. In general terms, this approach works by reconstructing the demographic rates required to project the distribution of abundances across demographic states from one time step to the next (Phillips et al., 2022). By explicitly modeling temporal variation in the demographic rates, we were able to take advantage of shared information across all time points simultaneously to constrain the

parameter estimates.

In the model as described below, movement is defined as the proportion of individuals that begin in one basin and end in the other basin over a given time interval. Moreover, recruitment is formulated as in situ per capita recruitment (i.e., new individuals appearing in a basin through birth in that basin per adult). By formulating in situ recruitment and movement as separate processes in the model, we endeavored to disentangle these processes through the model fitting. However, we acknowledge that any effort in model-based inference is subject to uncertainty and that the literal biological meaning of the demographic parameters should be interpreted with caution.

For a given time interval from $t-1$ to t, the population dynamics were projected as

$$\mathbf{x}_t = \mathbf{P}_{t-1}\ \mathbf{x}_{t-1} \tag{1}$$

where $\mathbf{P}_t$ is 4×4 a matrix of demographic rates at time t, and $\mathbf{x}_t$ is a 4×1 vector of relative abundances for a given stage (juveniles j; adults a) and basin (south s; north n):

$$\mathbf{x}_t = \begin{bmatrix} x_{j,s,t} \\ x_{a,s,t} \\ x_{j,n,t} \\ x_{a,n,t} \end{bmatrix}. \tag{2}$$

The projection matrix $\mathbf{P}_t$ can be expressed as

$$\mathbf{P}_t = \left[\begin{array}{c|c} \mathbf{W}_{s,t} & \mathbf{B}_{s\to n,t} \\ \hline \mathbf{B}_{n\to s,t} & \mathbf{W}_{n,t} \end{array}\right] \tag{3}$$

where $\mathbf{W}_{i,t}$ is a 2×2 matrix characterizing per capita contributions within basin i, and $\mathbf{B}_{i\to k,t}$ is a 2×2 matrix characterizing contributions from basin i to basin k. Within-basin contributions were modeled as

$$\mathbf{W}_{i,t} = \begin{bmatrix} \phi_{j,i,t}\ (1-\gamma_j)\ (1-\delta_{j,i,t}) & \rho_{i,t} \\ \phi_{j,i,t}\ \gamma_j\ (1-\delta_{a,i,t}) & \phi_{a,i,t}\ (1-\delta_{a,i,t}) \end{bmatrix} \tag{4}$$

where $\phi_{h,i,t}$ is the survival probability of stage-class h, γ_j is the proportion of surviving juveniles that transition into adults (i.e., the "stage-transition" probability), $\delta_{h,i,t}$ is the proportion of surviving individuals that move to the other basin, and $\rho_{i,t}$ is per capita recruitment. We modeled between-basin contributions as

$$\mathbf{B}_{i,t} = \begin{bmatrix} \phi_{j,i,t}\ (1-\gamma_j)\ \delta_{j,i,t} & 0 \\ \phi_{j,i,t}\ \gamma_j\ \delta_{a,i,t} & \phi_{a,i,t}\ \delta_{a,i,t} \end{bmatrix}. \tag{5}$$

For computational tractability, we fixed the stage-transition probability γ_j to a single value for both basins and through time; therefore, temporal variation in stage-transitions was implicitly incorporated into the time-varying survival probabilities.

To be biologically interpretable, survival, movement, and stage-transition probabilities must be constrained to between 0 and 1. Furthermore, probabilities of all possible fates for an individual beginning in a given state (i.e., basin $\times$ stage combination) must sum to 1. To accommodate these constraints, we modeled survival, movement, and stage-transitions in terms of latent transition rates (denoted ω_t^p for parameter p), from which we calculated the transition probabilities (i.e., $\phi_{h,i,t}$, γ_j, and $\delta_{h,i,t}$) projected over the interval between time steps (see Appendix A). This approach imposes an inverse relationship between the basin-specific movement probabilities for a given stage class, which is appropriate because only the net movement between basins manifests in the population dynamics. Our formulation first calculates survival, then stage transitions, and finally movement (Appendix A equation A5), which is reflected in the structure of equations 4 and 5.

We modeled temporal variation in recruitment ($\rho_{i,t}$) and latent transition rates (ω_t^p) as

$$\zeta_t^q \sim \text{Gaussian}\left(\zeta_{t-1}^q,\ \sigma_q\right) \text{Truncated}\left(0,\ \infty\right) \tag{6}$$

where ζ_t^q is the value for demographic rate q at time t, and σ_q is the standard deviation of the distribution. This approach results in autocorrelated changes in the demographic rates through time, since the contribution of equation 6 to the model likelihood (defined below) declines as the difference between ζ_t^q and ζ_{t-1}^q increases; the strength of this penalization against changes

in ζ_t^q declines as σ_q increases. We estimated a single value of σ_q for recruitment in both basins, and a single value for survival and movement of all state combinations, as these demographic processes respectively occurred on similar scales. Equation 6 was truncated from the left at zero (Stan Development Team, 2021) to ensure the demographic rates remained positive.

We used a Bayesian approach to estimate the parameters in the metapopulation model (equations 1 through 6) by fitting the model to site-level CPUE for each stage class h at each time step t, with a function $m(k)$ defined to map site k to basin i. Because we were interested in using CPUE to infer the relative abundance between basins, (rather than the absolute magnitude of CPUE), we divided CPUE by the global mean CPUE for model fitting (hereinafter "scaled CPUE"). The metapopulation model was formulated in terms of relative populations sizes in each basin, while site-level scaled CPUE is an index of population density. To account for this, we defined a variable κ_i to represent the relative sampling areas of the South Basin and the North Basin covered by the sampling sites, which were originally selected to represent the full distribution of the population throughout the lake. Specifically, we defined κ_s as the region of the South Basin excluding the region east of the chain of islands and south of site 135 (c. 17.5 km^2), and κ_n as the entire North Basin (c. 8.5 km^2) (Figure 1 A). This resulted in a 2:1 relative scaling of South vs. North Basin, or $\kappa_s = 2$ and $\kappa_b = 1$.

Using these definitions, we calculated the likelihood of scaled CPUE $y_{h,k,t}$ given a modeled relative abundance $x_{h,i,t}$ as

$$\mathcal{L} = \prod_{h,k,t} \text{Gaussian}\left(y_{h,k,t} \mid x_{h,m(k),t}/\kappa_{m(k)},\ \sigma_y\right), \tag{7}$$

with standard deviation σ_y representing "sampling error" that includes deviations of sites from the mean basin-level density. While other distributions might seem more appropriate for abundance data such as CPUE, we found that some common choices produced unsatisfactory fits to the observed data. Specifically, both log-normal and negative binomial distributions led to a flattening of the likelihood at high population densities (due to the variance scaling proportionally with mean), causing the model to be only weakly informed by the data at high densities.

Moreover, the multiplicative nature of population processes is already entailed in the population projection, and it is not obvious that variation in the distribution of individuals across sampling sites is best construed as a "count process". Therefore, we opted for a Gaussian likelihood. Because the model was parameterized in a way that ensured $x_{h,i,t}$ was non-negative, the posterior distribution of $x_{h,i,t}$ was also guaranteed to be non-negative.

We used gamma priors with shape parameter 1.5 for the initial values for demographic rates and standard deviations for time-varying rates and model likelihood. A gamma distribution with shape parameter of 1.5 has zero density at zero and is concave down as it approaches its mode, allowing the posterior to be arbitrarily close to zero while not being artificially drawn towards it. For most of the gamma priors, we used a scale parameter of 0.75 (implying a prior distribution mean of 2), which is a reasonable scale relative to the scaled CPUE data. However, we used a more conservative scale parameter of 3 (prior distribution mean of 0.5) for the initial values and standard deviation of transition rates to better constrain them on the latent scale. We used an exponential prior with a rate of 0.5 (prior distribution mean of 2) for initial relative abundances, which we chose as it was somewhat more diffuse than the gamma priors.

We fit the model using Stan 2.19 (Carpenter et al., 2017) run from R 4.0.3 (R Core Team, 2020), with the `rstan` package (Stan Development Team, 2018). We fit the model with 4 chains, 20000 iterations (10000 of warm-up and 10000 of sampling), thinning interval of 2 to retain a manageable number of samples, tree depth of 11, and "adapt delta" of 0.97. Convergence was assessed by the number of divergent transitions, the potential scale reduction factor ($\hat{R}$), the tail- and bulk-effective sample size, and trace plots for individual parameters (see Online Supplement: Model Assessment for further details). We used posterior medians as point estimates and quantile-based uncertainty intervals with coverage analogous to standard errors (16% and 84% quantiles for 68% coverage).

In addition to the full model, we also fit three reduced models to which it could be compared. First, we fit a model only including movement of adults ("adult movement"), because the demographic estimates from the full model implied negligible net movement of juveniles

between the basins. Second, we fit a model omitting movement entirely ("no movement"), allowing us to assess the contribution of movement to the model fit. Third, we fit a model with recruitment, survival, and adult movement fixed through time ("fixed rates"), allowing us to assess the contribution of temporal variation in demographic rates to the model fit. The fixed rates model omitted juvenile movement altogether, because the comparison of the full and adult movement models implied a negligible contribution of time-varying juvenile movement to the model fit (see Results). We assessed goodness-of-fit using three related metrics: the posterior median of the log-likelihood given by equation 7, the "widely applicable" information criterion (WAIC), and the "leave-one-out" cross validation information criterion (LOOIC). We calculated WAIC and LOOIC using the `loo` package (Vehtari et al., 2020).

Annual dynamics and sensitivity analysis

While we parameterized the model in terms of seasonal projections to accommodate the seasonal nature of the data (June and August censuses), we focused our analysis on the annual dynamics to better reflect the annual nature of spawning in this population and to circumvent interpretational issues arising from the unequal projection intervals within a year. Accordingly, we defined the annual projection matrix as

$$\mathbf{A}_y = \mathbf{P}_{t[y]+1}\mathbf{P}_{t[y]} \tag{8}$$

for year y and sequential time steps within that year $t[y]$ and $t[y]+1$, with the year defined to start with the June census. $\mathbf{A}_y$ projects the dynamics from June of one year to June of the next year. Because $\mathbf{P}_{t[y]}$ was defined through June of 2020, we only calculated $\mathbf{A}_y$ from 1991 through 2019.

We characterized the overall dynamics of the population in terms of the annual population growth rate λ_y, calculated as

$$\lambda_y = \frac{N_{y+1}}{N_y} = \frac{\mathbf{c}^\top \mathbf{A}_y \mathbf{x}_y}{\mathbf{c}^\top \mathbf{x}_y} \tag{9}$$

where N_y is the summed abundance across basins and life stages in June of year y and $\mathbf{c}$ is a 4×1

vector of ones (Caswell, 2001). Temporal variation in λ_y reflects both variation in the demographic rates and transient fluctuations due to non-equilibrium state distributions. Therefore, it is also informative to calculate the asymptotic population growth rate that would obtain under the equilibrium state distribution in a given time step, which is equal to real part of the leading eigenvalue of $\mathbf{A}_y$ (Caswell, 2001).

Both the transient and asymptotic population growth rates appeared to display periodic behavior for at least a portion of the three-decade time series (see Results). We quantified this putative periodicity by applying continuous wavelet transforms to the time series for the transient and asymptotic growth rates, on a log-scale (the results were similar for the raw values) and with no detrending. Wavelet transforms are a generalization of Fourier transforms, allowing the decomposition of the signal into periodic elements to be localized in time (Cazelles et al., 2008). Because our use of wavelet transforms was chiefly descriptive and applied to signals that were themselves the outputs of a statistical model, we did not attempt to apply formal statistical inference (i.e., hypothesis testing) to the wavelet decomposition. We conducted the wavelet analysis using the R package `WaveletComp` (Roesch et al., 2018), and for tractability we applied the wavelet transform to the posterior median of λ_y (rather than to multiple Markov chain samples). While the wavelet decomposition was conducted for periods up to the maximum period length (29 years), the signal associated with periods $>$10 years was very weak. So, for clarity of visualization we truncated the periodogram at 10 years.

We conducted a sensitivity analysis to evaluate the effect of perturbations in the demographic rates on the population growth rate, using the approach of Caswell (2007) that is applicable to transient dynamics (see Appendix B for relevant formulas). The sensitivity of the population growth rate with respect to a demographic parameter quantifies how much the growth rate would change in response to a perturbation in that demographic parameter. In order to compare across parameters of different magnitudes (which is particularly relevant in the present context with time-varying rates), it is common to calculate the proportional change in response to a proportional perturbation, otherwise known as the "elasticity" (Caswell, 2001). For each year,

we calculated the elasticity of the annual growth rate with respect to the demographic rates at each of the two intervals within that year. To simplify the presentation, we added together the elasticities for the intervals within a given year for each demographic parameter. We report the sensitivity analysis for both transient and asymptotic growth rates. Transient sensitivity analysis propagates perturbations in the demographic rates through time, such that transience due to non-equilibrium state distributions is attributed to the demographic parameters resulting in the non-equilibrium state distribution for a given time step (Caswell, 2007). Transient results were obtained by propagating each perturbation for a single time-step for each year, while approximate asymptotic results were obtained by propagating for 50 time-steps, which we confirmed was sufficiently long to exclude transient effects through visual comparison to shorter projections. The sensitivity analysis was performed for 2000 samples of the Markov chain generated during fitting of the full demographic model to propagate uncertainty parameter estimates.

Results

We used a stage-structured metapopulation model to characterize the population dynamics of Mývatn stickleback arising from temporal variation in movement, survival, and recruitment. To evaluate the degree to which the CPUE data provided meaningful information on the time-varying demographic rates, we compared the fits of alternative models with different combinations of fixed and time-varying rates. The model with all demographic rates fixed through time ("fixed rates") provided a much worse fit than any of the other models (Table 1; Figure 2), indicating that temporal variation in the demographic rates was important in accounting for the observed population dynamics. In contrast, the models including movement of adults only ("adult movement") and movement of both stage classes ("full model") provided nearly identical fits, indicating that there was no clear signature of differential movement of juveniles in the population dynamics. The model omitting movement altogether ("no movement") provided a somewhat worse fit to the data than the models including movement. Visually, this manifested

as slightly lower flexibility of the model without movement to track fluctuations in the data, even though the qualitative behavior was largely similar (Figure 2). The discrepancy between the models with and without movement was greatest for South Basin juveniles; allowing movement of adults from the North to South basins relaxed the constraints on inferred abundance of South Basin juveniles and thereby allowed a closer fit to the data. Hereafter, we present the results of the adult movement model, as it better characterized the data than the no movement and fixed rates models while being simpler than the full model.

The demographic rates fluctuated substantially over the study period, resulting in large changes in abundance. Per capita recruitment was of similar magnitude and modestly covaried between the two basins (Pearson correlation r = 0.50; Figure 3). However, South Basin recruitment was somewhat more variable, with a peak in 1991 being particularly striking. Survival probabilities covaried across stage classes within each basin (r = 0.88 and 0.84 for the South and North basins, respectively) and within stage classes between basins (r = 0.61 and 0.93 for juveniles and adults, respectively). For both stage classes in both basins, survival probabilities peaked in 2002-2003 prior to an extended decline until 2015, after which survival probabilities generally increased (Figure 4). However, survival probabilities of South Basin juveniles were lower than for the other classes throughout the time series, and this was especially true during the final decade. Figure 5 shows the inferred net movement between basins (rather than basin-specific movement probabilities), as this is most relevant to the observed population dynamics and thereby "visible" to the model when fit to the data (see Online Supplement: Movement Probabilities for further details). Net movement was generally low and punctuated by several "waves" of movement from north to south. While these waves of southward movement persisted throughout the time series, they were substantially larger prior to 2005 than afterwards. The direction of net movement was rarely northward and only of substantial magnitude in 2004, following a particularly large southward movement event.

We used both the transient and asymptotic growth rates to characterize the annual population dynamics. The transient growth rate quantified the dynamics as they actually occurred, including

fluctuations due to the non-equilibrium distribution of individuals across population states (i.e., basin $\times$ stage-class combinations). In contrast, the asymptotic growth rate assumed an equilibrium state-distribution at each time point and thereby isolated the direct long-term effects of the per capita demographic rates. Both the transient and asymptotic growth rates fluctuated substantially across the study period, indicating periods of rapid population growth and decline (Figure 6 A). Over the first two decades, the asymptotic growth rate was cyclic with a period of approximately 6 years (Figure 6 B). However, this was supplanted by fluctuations of lower-amplitude and higher-frequency in the last 10 years (Figure 6 A). The 6-year periodicity was weaker for the transient growth rate, which instead was dominated by two bouts of high-frequency fluctuations at the beginning and end of the study period. Together, these results indicate that there was a cyclic aspect to the large fluctuations of the Mývatn stickleback population, although the dynamics appear to have changed over the last decade. Furthermore, transience due to non-equilibrium state distributions reduced the apparent cyclicity in the realized population dynamics.

We assessed the potential contributions of each demographic rate to the population dynamics using elasticities, which quantified the proportional change in the population growth rate in response to proportional perturbations in the underlying demographic rates. Elasticities are shown for both the transient and asymptotic growth rates (Figure 7). Transient elasticities included indirect effects of changes in per capita demographic rates via changing distributions across basin $\times$ stage-class combinations, while the asymptotic elasticities only included direct effects of the per capita demographic rates. The elasticities fluctuated substantially through time. While these fluctuations were generally similar for the asymptotic and transient cases, the transient elasticities were more variable and strongly differed from the asymptotic elasticities in some individual years. This result mirrored the differences in the asymptotic and transient growth rates near the beginning and end of the study period (Figure 6). Furthermore, the asymptotic elasticities for juvenile survival and recruitment were identical within each basin, which is expected given their similar contributions to the population projection matrix (Caswell, 2001). However, this was not the case for the transient elasticities, which showed marked differences between juvenile survival

and recruitment within each basin in some years. In other words, the direct effects of juvenile survival and recruitment on the population growth rate were similar, but their indirect effects through changes in population state distribution differed in years when transience was especially pronounced.

Despite the large interannual variability in both asymptotic and transient elasticities, this variation was small relative to the overall contrasts between the different demographic rates (Figure 7). This indicates that the relative importance of different demographic processes remained broadly consistent throughout the study period. The elasticities were neutral or positive in most years for all demographic rates except for movement probabilities from the North to the South Basin, which were substantially negative in most years. The negative elasticities for southward movement indicated that conditions were demographically less favorable in the South than in the North Basin, such that increases in southward movement would reduce the population growth rate. Among the remaining demographic rates, the largest elasticities were for juvenile survival, recruitment, and adult survival in the North Basin, while the analogous rates for the South Basin were generally close to zero. This pattern was especially pronounced in the most recent years, coinciding with low survival (Figure 4) and adult abundance (Figure 1 B) in the South Basin. Together, these results show that the North Basin dominated the overall population dynamics, and this dominance increased towards the end of the study period.

Discussion

Despite the long-standing interest in population fluctuations, particularly those cyclic in character (Elton, 1924; Nicholson and Bailey, 1935), studies that decompose these dynamics into direct and indirect contributions from the underlying demographic rates are relatively rare (Fox and Gurevitch, 2000; Coulson et al., 2005; Koons et al., 2017). Using a metapopulation model with time-varying demographic rates fit to three decades of monitoring data (CPUE), we decomposed the population dynamics of threespine stickleback from Lake Mývatn into contributions from

recruitment, survival, and movement between the lake's North and South basins. Recruitment was only modestly synchronized between the two basins, whereas survival probabilities of adults were more-strongly synchronized, contributing to cyclic fluctuations in the lake-wide population with a period of approximately six years for most of the study period. Moreover, the two basins were coupled through movement of individuals, with the North Basin subsidizing the South Basin and playing an important role in the lake-wide dynamics. While the population dynamics were generally cyclic, they appeared to shift in the final decade towards fluctuations of lower amplitude and higher frequency. This shift was associated with a decline in lake-wide survival probabilities and reduced net movement. In addition to their direct effects, the time-varying demographic rates indirectly resulted in transient fluctuations in the population growth rate, partially obscuring the cyclic nature of the underlying dynamics. While we acknowledge the inherent limits of CPUE data for inferring population dynamics, particularly for movement and dispersal, our analysis provides a plausible characterization of the dynamics that could lead to the large spatiotemporal patterns in the observed data.

The fluctuations of the Mývatn stickleback population were best explained by changes in the per capita demographic rates, as opposed to being purely transient as would be embodied by a model with fixed demographic rates corresponding to basic life history characteristics (e.g., average lifespan or maturation rate; Caswell, 2001). Indeed, in the absence of time-varying demographic rates, the best-fitting model rapidly reached its equilibrium behavior of essentially constant population density. This finding is consistent with Wootton et al. (2005), who compared the dynamics of three different threespine stickleback populations in the United Kingdom (one riverine, one lacustrine, and one backwater) and found that only the backwater population had cyclic fluctuations. Such variation in the dynamics of different populations is contrary to what one would expect if the cyclicity were an inherent feature of threespine stickleback life-history. However, the lack of transient fluctuations arising directly from life history or demographic structure does not imply that transience was not important for the population dynamics. On the contrary, there were substantial transient effects on the realized population growth rate. These

transient features arose because of repeated perturbations of the demographic rates, which perpetually kept the population away from its equilibrium state distribution. While the dynamics of our model were locally linear and density-independent, our approach for inferring time-varying demographic rates can implicitly embody nonlinear and density-dependent dynamics (Ives and Dakos, 2012). It is possible that the time-varying demographic rates themselves were the manifestation of some transient phenomenon, such as overcompensatory density-dependence that could lead to sustained cycles under constant environmental conditions (e.g., May, 1974). This highlights the key point that transience must be defined with respect to some set of conditions under which a system can be characterized as "fixed" (Hastings, 2010), which is as much a feature of the observer as of the phenomenon being observed.

Uncovering the mechanistic basis for changes in the demographic rates is crucial for understanding the ecological and evolutionary relevance of population fluctuations. Our metapopulation model for Mývatn stickleback implies that processes both lake-wide and specific to each basin are likely to contribute. For example, the broadly synchronized survival probabilities across the lake, especially for adults, suggest a lake-wide driver. While several possibilities exist, a likely candidate is predation from salmonids such as Arctic charr and brown trout. Arctic charr in particular are widely distributed and disperse extensively throughout the lake (Guðbergsson, 1991, 2004), which could induce synchronous fluctuations in stickleback survival. Avian predators may also be important drivers of temporal variation in survival, although they tend to be more localized (Einarsson et al., 2004) and therefore do not obviously account for similarities between the two basins. Predation-induced synchrony among sub-populations has been observed in other metapopulations and may be quite common in cases where predators are highly mobile relative to their prey (Ims and Andreassen, 2000; Gilg et al., 2009). In contrast to survival, per capita recruitment was less correlated between the two basins, implying that it was driven in part by factors unique to each. The two basins differ substantially in their substrates, bathymetry, and water chemistry (Einarsson et al., 2004), which in turn translates to differences in invertebrate communities (Bartrons et al., 2015) that serve as key food sources for threespine stickleback.

Food availability could influence adult fecundity or survival of recently hatched juveniles, both of which would manifest as variation in per capita recruitment in our model. Infection by the tapeworm *Schistocephalus solidus* could also account for spatiotemporal variation in fecundity (Heins et al., 2010; Heins, 2012), which is the subject of ongoing research in the Mývatn population. Moreover, our model indicates a shift in the dynamics of the stickleback population over the past decade, with the 6-periodicity dominant in the first two-thirds of the study period giving way to more irregular high-frequency fluctuations. While the basis for this change is unclear, it could be connected to a shift in the Arctic charr population towards a more adult-dominated age distribution (Phillips et al., 2022). However, other aspects of the Mývatn ecosystem may have changed over this time period as well, which is a topic of ongoing study.

In addition to the ecological perspective of population demography and spatial heterogeneity, our analyses have implications for evolutionary processes over space and time. Threespine stickleback provide some of the most prominent examples of rapid evolution, adaptive divergence, and ecological speciation (reviewed in Hendry et al., 2013). In Mývatn, the distribution of the threespine stickleback population across two ecologically distinct basins with differentiation in demographic rates could set the stage for adaptive divergence. Previous work from Mývatn has identified spatial variation in feeding morphology and defensive traits (Millet et al., 2013). For example, dorsal spines tend to be longer in the North Basin than in the South Basin, which might reflect elevated predation risk (Hoogland et al., 1956; Reimchen and Nosil, 2002). However, population-genetic studies have provided mixed evidence for genetic differentiation and clear evidence of extensive gene flow across the lake (Ólafsdóttir et al., 2007; Millet et al., 2013), which is consistent with the inference from our metapopulation model that the two basins are dynamically coupled through movement. Nonetheless, if differences in natural selection between the basins are sufficiently strong, it is plausible that this could result in phenotypic differentiation even in the absence of clear population-genetic structure (Räsänen and Hendry, 2008). The apparent phenotypic variation between the two basins could also be explained by phenotypic plasticity, which theoretical work suggests may be favored in metapopulations with strong cou-

pling through movement (Sultan and Spencer, 2002). Moreover, the large temporal variation in survival and recruitment may set the stage for fluctuating selection (Siepielski et al., 2009), which in turn could lead to rapid evolutionary changes in traits associated with the underlying demographic rates. Per capita population growth rates are tightly associated with evolutionary fitness, and previous studies have successfully linked fluctuating population growth rates to rapid evolutionary change in other populations (Coulson and Tuljapurkar, 2008; Engen et al., 2014; de Vries and Caswell, 2019). A challenge for future work is to characterize how these eco-evolutionary processes manifest in space (Hanski, 2012; Brunner et al., 2019).

In conclusion, we fit a stage-structured metapopulation model to a 29-year times series of threespine stickleback abundance in the heterogeneous and productive Lake Mývatn, Iceland. Together, our results show how cyclic fluctuations can be explained by the combination of synchronized demographic rates and spatial coupling through movement. Moreover, we show how transient shifts in the distribution of individuals across population states can lead to short-term deviations from long-term cyclic dynamics. Our analysis provides important context for future efforts to decompose the fluctuations of wild metapopulations into contributions from time-varying demographic rates.

Appendix A: Transition rates

We parameterized latent transition rate matrices for mortality ($\mathbf{\Omega}_t^{\mu}$), stage-transition ($\mathbf{\Omega}^{\gamma}$), and movement ($\mathbf{\Omega}_t^{\delta}$) as:

$$\mathbf{\Omega}_t^{\mu} = \left[\begin{array}{cc|cc} -\omega_t^{\phi_{j,s}} & 0 & 0 & 0 \\ 0 & -\omega_t^{\phi_{a,s}} & 0 & 0 \\ \hline 0 & 0 & -\omega_t^{\phi_{j,n}} & 0 \\ 0 & 0 & 0 & -\omega_t^{\phi_{a,n}} \end{array}\right] \tag{A1}$$

$$\mathbf{\Omega}^{\gamma} = \left[\begin{array}{cc|cc} -\omega^{\gamma_j} & 0 & 0 & 0 \\ \omega^{\gamma_j} & 0 & 0 & 0 \\ \hline 0 & 0 & -\omega^{\gamma_j} & 0 \\ 0 & 0 & \omega^{\gamma_j} & 0 \end{array}\right] \tag{A2}$$

$$\mathbf{\Omega}_t^{\delta} = \left[\begin{array}{cc|cc} -\omega_t^{\delta_{j,s}} & 0 & \omega_t^{\delta_{j,n}} & 0 \\ 0 & -\omega_t^{\delta_{a,s}} & 0 & \omega_t^{\delta_{a,n}} \\ \hline \omega_t^{\delta_{j,s}} & 0 & -\omega_t^{\delta_{j,n}} & 0 \\ 0 & \omega_t^{\delta_{a,s}} & 0 & -\omega_t^{\delta_{a,n}} \end{array}\right] \tag{A3}$$

Note that mortality implicitly entails transition to a "death state" that is omitted for succinctness, as dead individuals do not contribute to future transitions. For each transition matrix $\mathbf{\Omega}_t^{\alpha}$, we then calculated the probability of transitioning as

$$\mathbf{\Psi}_t^{\alpha} = e^{\mathbf{\Omega}_t^{\alpha}} \tag{A4}$$

which is the solution to the differential equation associated with the Markov process specified by $\mathbf{\Omega}_t^{\alpha}$ with initial condition equal to the 4×4 identity matrix (Yang, 2006). The unequal projection interval duration from June-August and August-June was handled implicitly by the time-varying rates, which proved more computationally stable than explicitly accounting for the projection interval duration in equation A4.

The transition probability matrix was calculated as

$$\mathbf{P}_t = \mathbf{\Psi}_t^{\delta}\ \mathbf{\Psi}^{\gamma}\ \mathbf{\Psi}_t^{\mu}. \tag{A5}$$

The order of multiplication implies that proportional survival is calculated first, followed by stage-transitions, and finally movement, resulting in the configuration of transition probabilities given in equations 4 and 5. In principle, we could have included all of the demographic transitions in a single transition matrix, which would imply that all of the transition processes occurred simultaneously. However, modeling the different transition processes sequentially facilitated interpretation of the resulting transition probabilities (i.e., the matrix elements in equations 4 and 5), as they would only pertain to a single type of demographic transition rather than multiple transition processes occurring simultaneously. This also facilitated convergence of the MCMC algorithm during model fitting, for much the same reasons.

Appendix B: Sensitivity analysis

We used the method of Caswell (2007) to calculate the elasticities (proportional sensitivities) of the annual transient population growth rate λ_y with respect to perturbations in the seasonal demographic rates. It was convenient to perform the calculations using the logarithm of λ_y, commonly denoted r_y. This parameter is related to total population size N_y by the expression

$$r_y = \log\left(N_{y+1}\right) - \log\left(N_y\right). \tag{B1}$$

Note that

$$\frac{\mathrm{d}\lambda_y}{\mathrm{d}\theta} = \lambda_y \frac{\mathrm{d}r_y}{\mathrm{d}\theta} \tag{B2}$$

where $\frac{\mathrm{d}\lambda_y}{\mathrm{d}\theta}$ can generically be interpreted as the sensitivity of λ_y with respect to perturbations in a single parameter θ. The elasticity of λ_y is then defined as

$$\frac{\theta}{\lambda_y}\frac{\mathrm{d}\lambda_y}{\mathrm{d}\theta} = \theta \frac{\mathrm{d}r_y}{\mathrm{d}\theta}. \tag{B3}$$

The multiplication of $\frac{\mathrm{d}r_y}{\mathrm{d}\theta}$ by θ implies proportional perturbations in θ. Therefore, the sensitivity of r_y with respect to proportional perturbations in θ equals the elasticity of λ_y. This deduction is essentially a restatement of logarithmic relationship of λ_y and r_y, along with the properties of logarithmic derivatives.

The transient sensitivity of r_y with respect to perturbations in demographic parameters is defined as

$$\frac{\mathrm{d}r_y}{\mathrm{d}\boldsymbol{\theta}_y^\top} = \frac{\mathbf{c}^\top}{N_{y+1}}\frac{\mathrm{d}\mathbf{x}_{y+1}}{\mathrm{d}\boldsymbol{\theta}_{y+1}^\top} - \frac{\mathbf{c}^\top}{N_y}\frac{\mathrm{d}\mathbf{x}_y}{\mathrm{d}\boldsymbol{\theta}_y^\top} \tag{B4}$$

where $\boldsymbol{\theta}_y$ is a vector of demographic parameters in year y, $\mathbf{x}_y$ is a 4×1 vector of abundances in each state, $\mathbf{c}$ is a 4×1 vector of ones, and "d" is the derivative operator. We were interested in the sensitivity of r_y with respect to proportional perturbations in the seasonal demographic rates, which are connected to $\mathbf{x}_y$ through the annual population projection matrix $\mathbf{A}_y$ as defined in equation 8. If $\boldsymbol{\theta}_y$ contains the seasonal demographic rates (i.e., the collective elements of $\mathbf{P}_{t[y]}$

and $\mathbf{P}_{t[y]+1}$) and $\boldsymbol{\epsilon}_y$ is a vector of proportional perturbations in $\boldsymbol{\theta}_y$, then

$$\frac{\mathrm{d}\mathbf{x}_{y+1}}{\mathrm{d}\boldsymbol{\theta}_{y+1}^{\top}} = \mathbf{A}_y \frac{\mathrm{d}\mathbf{x}_y}{\mathrm{d}\boldsymbol{\theta}_y^{\top}} + \left(\mathbf{x}_y^{\top} \otimes \mathbf{I}_c\right) \frac{\mathrm{d}\mathrm{vec}\mathbf{A}_y}{\mathrm{d}\boldsymbol{\epsilon}_y^{\top}} \mathrm{diag}\boldsymbol{\epsilon}_y \tag{B5}$$

where $\mathbf{I}_c$ is the $c \times c$ identity matrix with c as the length of the parameter vector θ_y, $\otimes$ is the Kroenecker product operator, "vec" is an operator that creates a vector by stacking columns of the operand matrix, and "diag" is an operator that creates a square matrix with the operand vector on the diagonal and zeros elsewhere. Defining an initial population size distribution $\mathbf{x}_0$ that is independent of the demographic parameters implies that $\frac{\mathrm{d}\mathbf{x}_0}{\mathrm{d}\boldsymbol{\theta}_0^{\top}} = \mathbf{0}$. Using this initial condition, the sensitivities can then be calculated by iterating equations B4 and B5 for each year, with perturbations $\boldsymbol{\epsilon}_y$ proportional (or equal) to the parameter vector $\boldsymbol{\theta}_y$. Asymptotic results can be obtained by iterating B5 many times for a given year, which eliminates the dependence on the initial values such that each year can be treated independently.

Acknowledgments

The data used in this manuscript were collected as part of a long-term monitoring program conducted by the Mývatn Research Station and Hólar University. We would like to thank Asgrimur Guðmundsson, who helped designed the monitoring program. We would also like to thank Antoine Millet, who contributed to data collection for many seasons, along with many other field assistants. This work was supported by RANNIS GOE-195571-052 to BKK and US-NSF LTREB DEB-1556208 to ARI.

Statement of Authorship

AE led long-term data collection with contributions from BKK, KR, JSP, and KS. JSP and ARI designed the analysis, and JSP performed the analysis. JSP wrote the first draft of the manuscript, and all authors contributed to subsequent revisions and final approval.

Data and Code Accessibility

The data used in this manuscript are available on Dryad (doi:10.5061/dryad.5x69p8d62) and the code for performing the analyses are available on Zenodo (doi:10.5281/zenodo.6678898).

Literature Cited

Abbott, K. C. 2011. A dispersal-induced paradox: synchrony and stability in stochastic metapopulations. Ecology Letters 14:1158–1169.

Baker, J., D. Heins, S. Foster, and R. King. 2008. An overview of life-history variation in female threespine stickleback. Behaviour 145:579–602.

Baker, J., M. Wund, D. Heins, R. King, M. Reyes, and S. Foster. 2015. Life-history plasticity in female threespine stickleback. Heredity 115:322–334.

Bartrons, M., A. Einarsson, R. L. Nobre, C. M. Herren, K. C. Webert, S. Brucet, S. R. Olafsdóttir, and A. R. Ives. 2015. Spatial patterns reveal strong abiotic and biotic drivers of zooplankton community composition in Lake Mývatn, Iceland. Ecosphere 6:1–20.

Bjørnstad, O. N., R. A. Ims, and X. Lambin. 1999. Spatial population dynamics: analyzing patterns and processes of population synchrony. Trends in Ecology & Evolution 14:427–432.

Bonnet, T., M. B. Morrissey, A. Morris, S. Morris, T. H. Clutton-Brock, J. M. Pemberton, and L. E. Kruuk. 2019. The role of selection and evolution in changing parturition date in a red deer population. PLoS Biology 17:e3000493.

Brunner, F. S., J. A. Deere, M. Egas, C. Eizaguirre, and J. A. Raeymaekers. 2019. The diversity of eco-evolutionary dynamics: Comparing the feedbacks between ecology and evolution across scales. Functional Ecology 33:7–12.

Carpenter, B., A. Gelman, M. D. Hoffman, D. Lee, B. Goodrich, M. Betancourt, M. Brubaker, J. Guo, P. Li, and A. Riddell. 2017. Stan: A probabilistic programming language. Journal of Statistical Software 76.

Caswell, H. 2001. Matrix Population Models: Construction, Analysis, and Interpretation. 2nd edn. Sinauer Associates.

———. 2007. Sensitivity analysis of transient population dynamics. Ecology Letters 10:1–15.

Caswell, H., and M. G. Neubert. 2005. Reactivity and transient dynamics of discrete-time ecological systems. Journal of Difference Equations and Applications 11:295–310.

Cazelles, B., M. Chavez, D. Berteaux, F. Ménard, J. O. Vik, S. Jenouvrier, and N. C. Stenseth. 2008. Wavelet analysis of ecological time series. Oecologia 156:287–304.

Coulson, T., T. Benton, P. Lundberg, S. Dall, and B. Kendall. 2006. Putting evolutionary biology back in the ecological theatre: a demographic framework mapping genes to communities. Evolutionary Ecology Research 8:1155–1171.

Coulson, T., J.-M. Gaillard, and M. Festa-Bianchet. 2005. Decomposing the variation in population growth into contributions from multiple demographic rates. Journal of Animal Ecology 74:789–801.

Coulson, T., and S. Tuljapurkar. 2008. The dynamics of a quantitative trait in an age-structured population living in a variable environment. The American Naturalist 172:599–612.

de Vries, C., and H. Caswell. 2019. Stage-structured evolutionary demography: linking life histories, population genetics, and ecological dynamics. The American Naturalist 193:545–559.

Diller, L. V., K. A. Hamm, D. A. Early, D. W. Lamphear, K. M. Dugger, C. B. Yackulic, C. J. Schwarz, P. C. Carlson, and T. L. McDonald. 2016. Demographic response of northern spotted owls to barred owl removal. The Journal of Wildlife Management 80:691–707.

Einarsson, A., A. Garðarsson, G. M. Gíslason, and A. R. Ives. 2002. Consumer–resource interactions and cyclic population dynamics of *Tanytarsus gracilentus* (Diptera: Chironomidae). Journal of Animal Ecology 71:832–845.

Einarsson, A., and E. B. Örnólfsdóttir. 2004. Long-term changes in benthic Cladocera populations in Lake Mývatn, Iceland. Aquatic Ecology 38:253–262.

Einarsson, A., G. Stefánsdóttir, H. Jóhannesson, J. S. Olafsson, G. M. Gíslason, I. Wakana, G. Guðbergsson, and A. Garðarsson. 2004. The ecology of Lake Mývatn and the River Laxá: variation in space and time. Aquatic Ecology 38:317–348.

Ellner, S. P., M. A. Geber, and N. G. Hairston Jr. 2011. Does rapid evolution matter? Measuring the rate of contemporary evolution and its impacts on ecological dynamics. Ecology Letters 14:603–614.

Elton, C. S. 1924. Periodic fluctuations in the numbers of animals: their causes and effects. Journal of Experimental Biology 2:119–163.

Engen, S., T. Kvalnes, and B.-E. Sæther. 2014. Estimating phenotypic selection in age-structured populations by removing transient fluctuations. Evolution 68:2509–2523.

Fox, G. A., and J. Gurevitch. 2000. Population numbers count: tools for near-term demographic analysis. The American Naturalist 156:242–256.

Fujiwara, M., and H. Caswell. 2002. Estimating population projection matrices from multi-stage mark–recapture data. Ecology 83:3257–3265.

Garðarsson, A. 1979. Waterfowl populations of Lake Mỳvatn and recent changes in numbers and food habits. Oikos pages 250–270.

Garðarsson, A., A. Einarsson, G. M. Gíslason, T. Hrafnsdóttir, H. R. Ingvason, E. Jónsson, and J. S. Olafsson. 2004. Population fluctuations of chironomid and simuliid Diptera at Mývatn in 1977–1996. Aquatic Ecology 38:209–217.

Gilg, O., B. Sittler, and I. Hanski. 2009. Climate change and cyclic predator–prey population dynamics in the high Arctic. Global Change Biology 15:2634–2652.

Gíslason, G. M., A. Guðmundsson, and A. Einarsson. 1998. Population densities of the three-spined stickleback (*Gasterosteus aculeatus L.*) in a shallow lake. Internationale Vereinigung für theoretische und angewandte Limnologie: Verhandlungen 26:2244–2250.

Goldwyn, E. E., and A. Hastings. 2008. When can dispersal synchronize populations? Theoretical Ppopulation Biology 73:395–402.

Guðbergsson, G. 1991. Silungsrannsóknir í Mývatni 1986–1990. Tech. rep., Institute of Freshwater Fisheries (Iceland).

———. 2004. Arctic charr in Lake Mývatn: the centennial catch record in the light of recent stock estimates. Aquatic Ecology 38:271–285.

Guðmundsson, A. 1996. Hornsíli í Mývatni. University of Iceland M.Sc. thesis.

Hanski, I. 1998. Metapopulation dynamics. Nature 396:41–49.

———. 2012. Eco-evolutionary dynamics in a changing world. Annals of the New York Academy of Sciences 1249:1–17.

Hastings, A. 2010. Timescales, dynamics, and ecological understanding. Ecology 91:3471–3480.

Heins, D. C. 2012. Fecundity compensation in the three-spined stickleback *Gasterosteus aculeatus* infected by the diphyllobothriidean cestode *Schistocephalus solidus*. Biological Journal of the Linnean Society 106:807–819.

Heins, D. C., J. A. Baker, M. A. Toups, and E. L. Birden. 2010. Evolutionary significance of fecundity reduction in threespine stickleback infected by the diphyllobothriidean cestode *Schistocephalus solidus*. Biological Journal of the Linnean Society 100:835–846.

Hendry, A. P., C. L. Peichel, B. Matthews, J. W. Boughman, and P. Nosil. 2013. Stickleback research: the now and the next. Evolutionary Ecology Research 15:111–141.

Hoogland, R., D. Morris, and N. Tinbergen. 1956. The spines of sticklebacks (*Gasterosteus* and *Pygosteus*) as means of defence against predators (*Perca* and *Esox*). Behaviour pages 205–236.

Hoy, S. R., D. R. MacNulty, D. W. Smith, D. R. Stahler, X. Lambin, R. O. Peterson, J. S. Ruprecht, and J. A. Vucetich. 2020. Fluctuations in age structure and their variable influence on population growth. Functional Ecology 34:203–216.

Hunter, C. M., H. Caswell, M. C. Runge, E. V. Regehr, S. C. Amstrup, and I. Stirling. 2010. Climate change threatens polar bear populations: a stochastic demographic analysis. Ecology 91:2883–2897.

Ims, R. A., and H. P. Andreassen. 2000. Spatial synchronization of vole population dynamics by predatory birds. Nature 408:194–196.

Ives, A. R., and V. Dakos. 2012. Detecting dynamical changes in nonlinear time series using locally linear state-space models. Ecosphere 3:1–15.

Ives, A. R., A. Einarsson, V. A. Jansen, and A. Garðarsson. 2008. High-amplitude fluctuations and alternative dynamical states of midges in Lake Mývatn. Nature 452:84–87.

Karvonen, A., B. K. Kristjánsson, S. Skúlason, M. Lanki, C. Rellstab, and J. Jokela. 2013. Water temperature, not fish morph, determines parasite infections of sympatric Icelandic threespine sticklebacks (*Gasterosteus aculeatus*). Ecology and Evolution 3:1507–1517.

Kendall, B. E., O. N. Bjørnstad, J. Bascompte, T. H. Keitt, and W. F. Fagan. 2000. Dispersal, environmental correlation, and spatial synchrony in population dynamics. The American Naturalist 155:628–636.

Koons, D. N., T. W. Arnold, and M. Schaub. 2017. Understanding the demographic drivers of realized population growth rates. Ecological Applications 27:2102–2115.

Koons, D. N., D. T. Iles, M. Schaub, and H. Caswell. 2016. A life-history perspective on the demographic drivers of structured population dynamics in changing environments. Ecology Letters 19:1023–1031.

Liebhold, A., W. D. Koenig, and O. N. Bjørnstad. 2004. Spatial synchrony in population dynamics. Annu. Rev. Ecol. Evol. Syst. 35:467–490.

Maciejewski, M. F., C. Jiang, Y. E. Stuart, and D. I. Bolnick. 2020. Microhabitat contributes to microgeographic divergence in threespine stickleback. Evolution 74:749–763.

May, R. M. 1974. Biological populations with nonoverlapping generations: stable points, stable cycles, and chaos. Science 186:645–647.

Millet, A., B. K. Kristjánsson, A. Einarsson, and K. Räsänen. 2013. Spatial phenotypic and genetic structure of threespine stickleback (*Gasterosteus aculeatus*) in a heterogeneous natural system, Lake Mývatn, iceland. Ecology and Evolution 3:3219–3232.

Moran, P. A. 1953. The statistical analysis of the Canadian lynx cycle. Australian Journal of Zoology 1:291–298.

Nicholson, A. J., and V. A. Bailey. 1935. The Balance of Animal Populations—Part I. Proceedings of the Zoological Society of London 105:551–598.

Ólafsdóttir, G., S. Snorrason, and M. Ritchie. 2007. Postglacial intra-lacustrine divergence of icelandic threespine stickleback morphs in three neovolcanic lakes. Journal of Evolutionary Biology 20:1870–1881.

Ozgul, A., D. Z. Childs, M. K. Oli, K. B. Armitage, D. T. Blumstein, L. E. Olson, S. Tuljapurkar, and T. Coulson. 2010. Coupled dynamics of body mass and population growth in response to environmental change. Nature 466:482–485.

Phillips, J. S., G. Guðbergsson, and A. R. Ives. 2022. Opposing trends in survival and recruitment slow the recovery of a historically overexploited fishery. Canadian Journal of Fisheries and Aquatic Sciences .

R Core Team. 2020. R: A Language and Environment for Statistical Computing. R Foundation for Statistical Computing, Vienna, Austria.

Ranta, E., V. Kaitala, J. Lindström, and H. Linden. 1995. Synchrony in population dynamics. Proceedings of the Royal Society of London. Series B: Biological Sciences 262:113–118.

Räsänen, K., and A. P. Hendry. 2008. Disentangling interactions between adaptive divergence and gene flow when ecology drives diversification. Ecology Letters 11:624–636.

Reimchen, T., and P. Nosil. 2002. Temporal variation in divergent selection on spine number in threespine stickleback. Evolution 56:2472–2483.

Roesch, A., H. Schmidbauer, and M. A. Roesch. 2018. Package 'WaveletComp' version 1.1.

Rosenzweig, M. L., and R. H. MacArthur. 1963. Graphical representation and stability conditions of predator-prey interactions. The American Naturalist 97:209–223.

Siepielski, A. M., J. D. DiBattista, and S. M. Carlson. 2009. It's about time: the temporal dynamics of phenotypic selection in the wild. Ecology Letters 12:1261–1276.

Singkam, A. R., and A. D. MacColl. 2019. Resources are more important than predation in driving the size at maturation of freshwater threespine stickleback (*Gasterosteus aculeatus*). Evolutionary Ecology Research 20:265–278.

Snyder, R. J. 1991. Migration and life histories of the threespine stickleback: evidence for adaptive variation in growth rate between populations. Environmental Biology of Fishes 31:381–388.

Stan Development Team. 2018. Rstan: the R interface to Stan. R package version 2.17.3.

———. 2021. Stan Modeling Language Users Guide and Reference Manual version 2.28.

Sultan, S. E., and H. G. Spencer. 2002. Metapopulation structure favors plasticity over local adaptation. The American Naturalist 160:271–283.

Taylor, L. U., B. K. Woodworth, B. K. Sandercock, and N. T. Wheelwright. 2018. Demographic drivers of collapse in an island population of tree swallows. The Condor: Ornithological Applications 120:828–841.

Twombly, S. 1994. Comparative demography and population dynamics of two coexisting copepods in a Venezuelan floodplain lake. Limnology and Oceanography 39:234–247.

Vehtari, A., J. Gabry, M. Magnusson, Y. Yao, P.-C. Bürkner, T. Paananen, and A. Gelman. 2020. loo: Efficient leave-one-out cross-validation and waic for bayesian models. R package version 2.4.0.

White, P., J. E. Bruggeman, and R. A. Garrott. 2007. Irruptive population dynamics in yellowstone pronghorn. Ecological Applications 17:1598–1606.

Wootton, R. J., C. E. Adams, and M. J. Attrill. 2005. Empirical modelling of the population dynamics of a small population of the threespine stickleback, *Gasterosteus aculeatus*. Environmental Biology of Fishes 74:151–161.

Yang, Z. 2006. Computational molecular evolution. Oxford University Press Oxford.

Zeng, Z., R. M. Nowierski, M. L. Taper, B. Dennis, and W. P. Kemp. 1998. Complex population dynamics in the real world: modeling the influence of time-varying parameters and time lags. Ecology 79:2193–2209.

Tables

Table 1: Comparison of model fits.

Model	Log-likelihood	WAIC	ΔWAIC	LOOIC	ΔLOOIC
full model	-1486	3174	0	3173	0
adult movement	-1485	3174	0	3175	2
no movement	-1502	3196	22	3194	21
fixed rates	-1721	3463	290	3463	290

Note: Log-likelihood is calculated as the posterior median

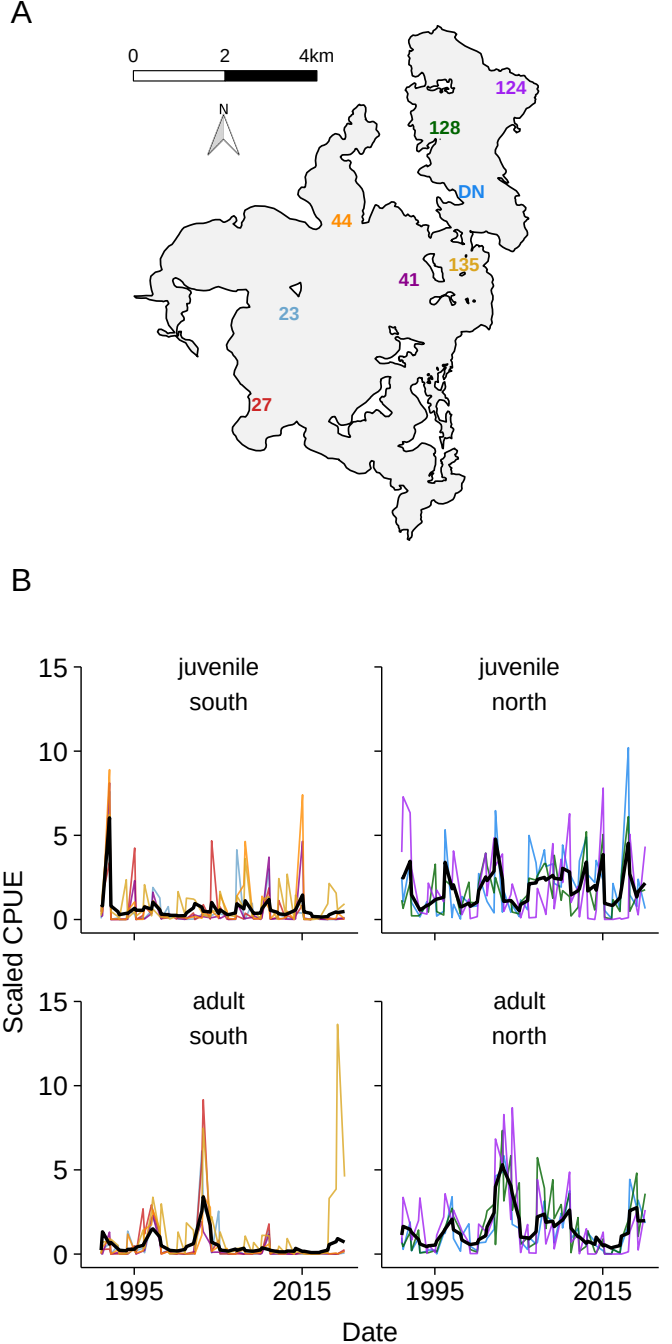
A
0
2
4km
N
124
128
DN
44
135
41
23
27
B
juvenile
south
juvenile
north
adult
south
adult
north
15
10
5
0
Scaled CPUE
1995
2015
Date

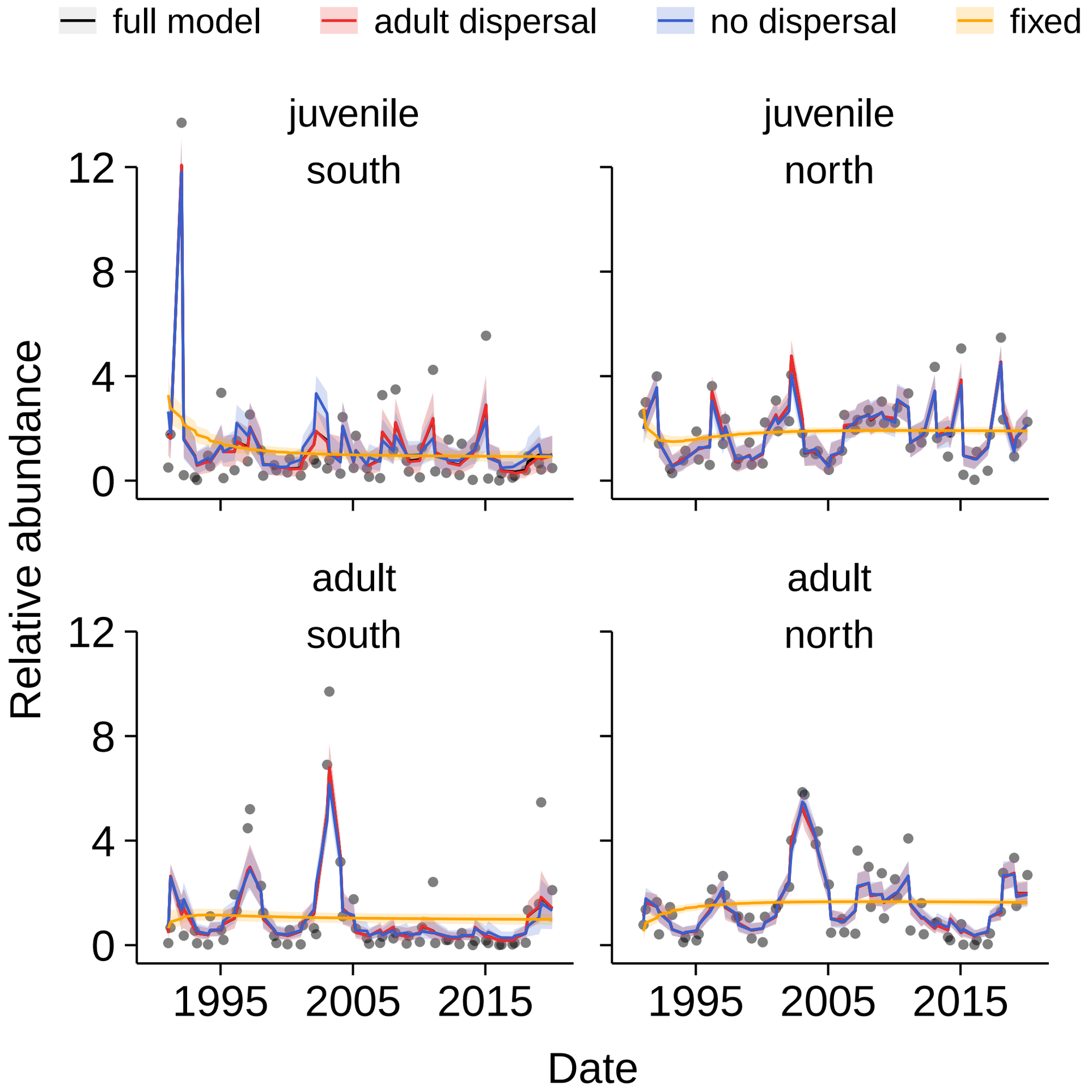
full model
adult dispersal
no dispersal
fixed
juvenile
south
juvenile
north
adult
south
adult
north
Relative abundance
0
4
8
12
1995
2005
2015
Date

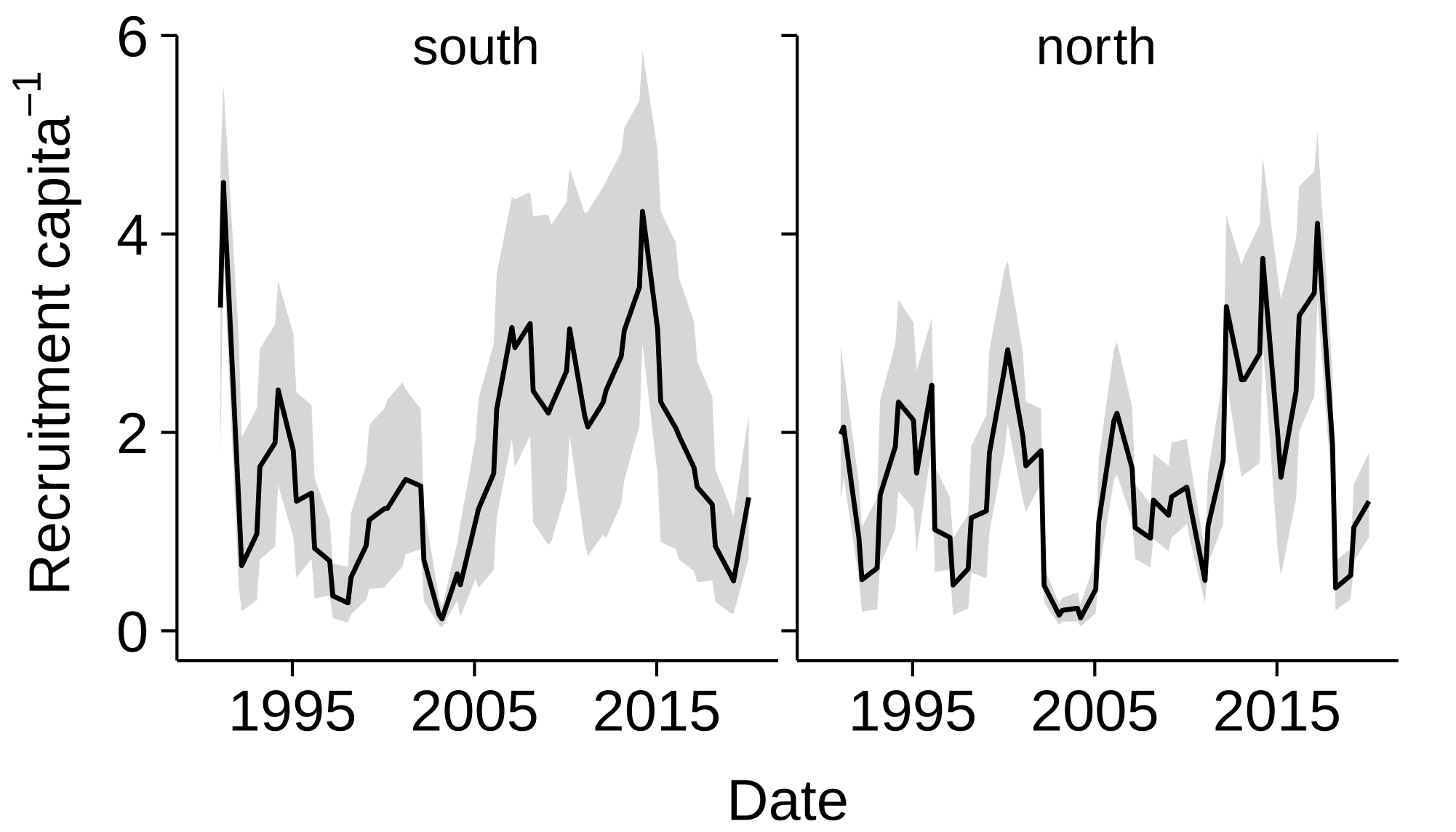
south
north
Recruitment capita^{-1}
0
2
4
6
1995
2005
2015
Date

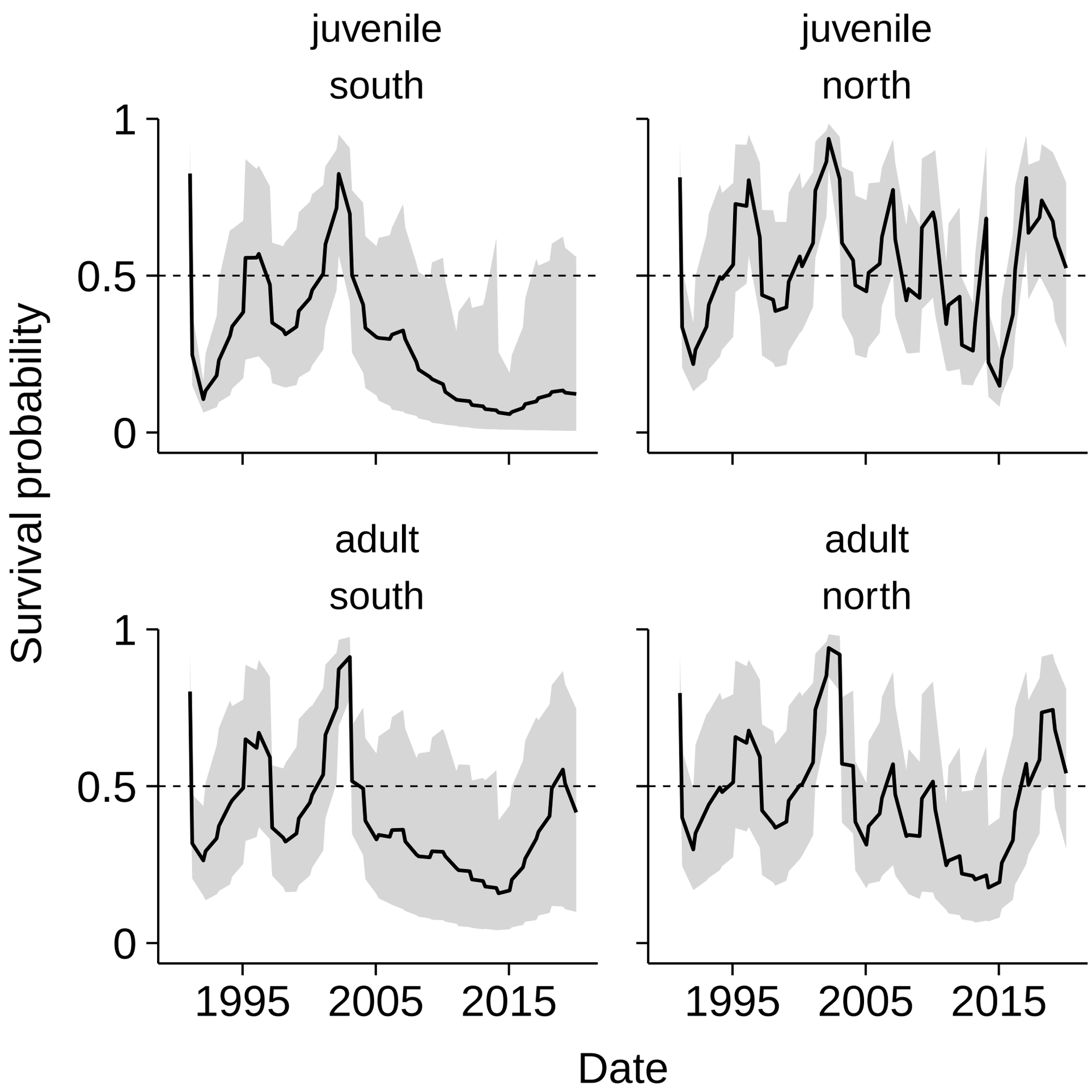
juvenile
south
juvenile
north
adult
south
adult
north
Survival probability
1
0.5
0
1995
2005
2015
Date

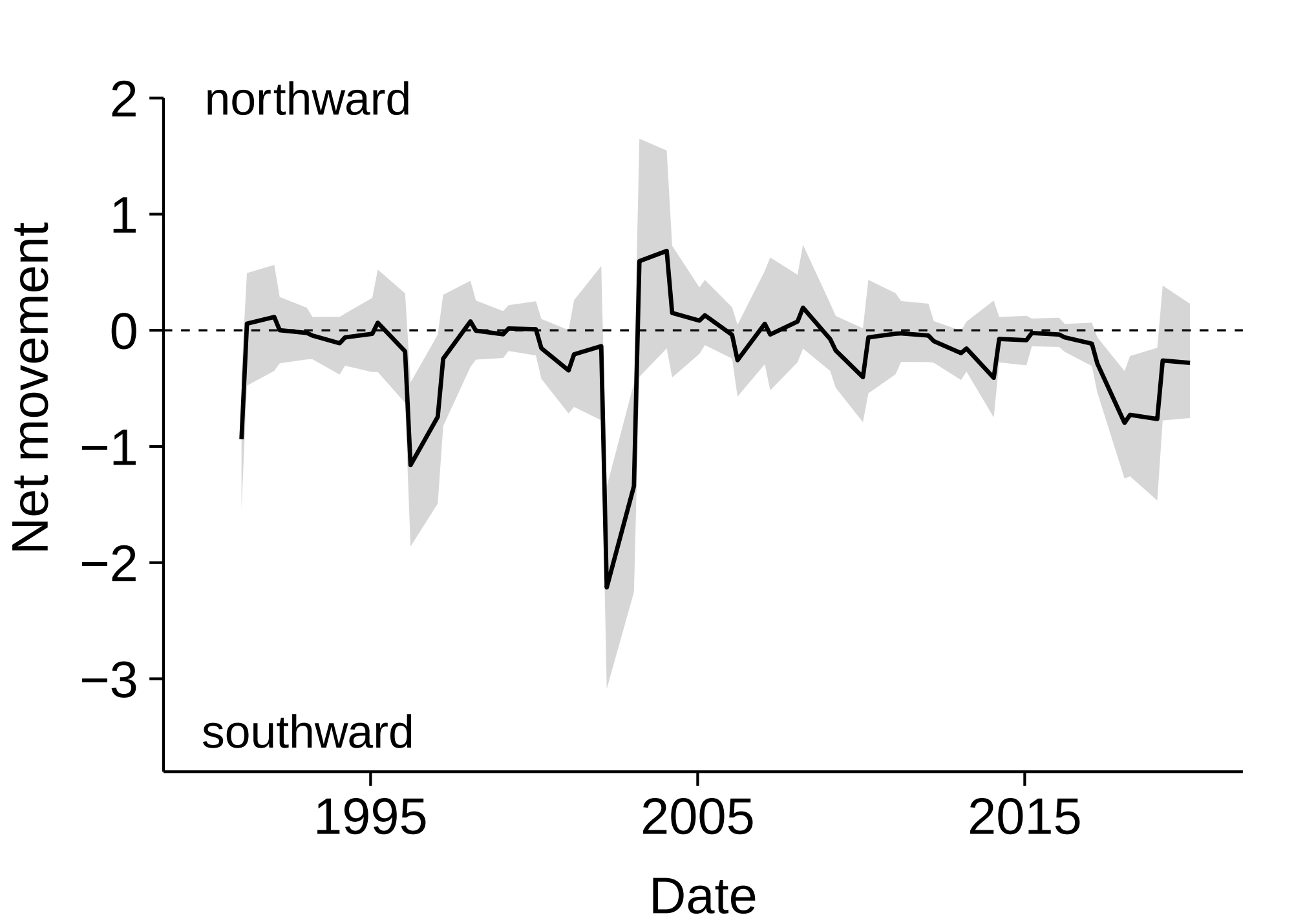
northward
southward
Net movement
2
1
0
−1
−2
−3
1995
2005
2015
Date

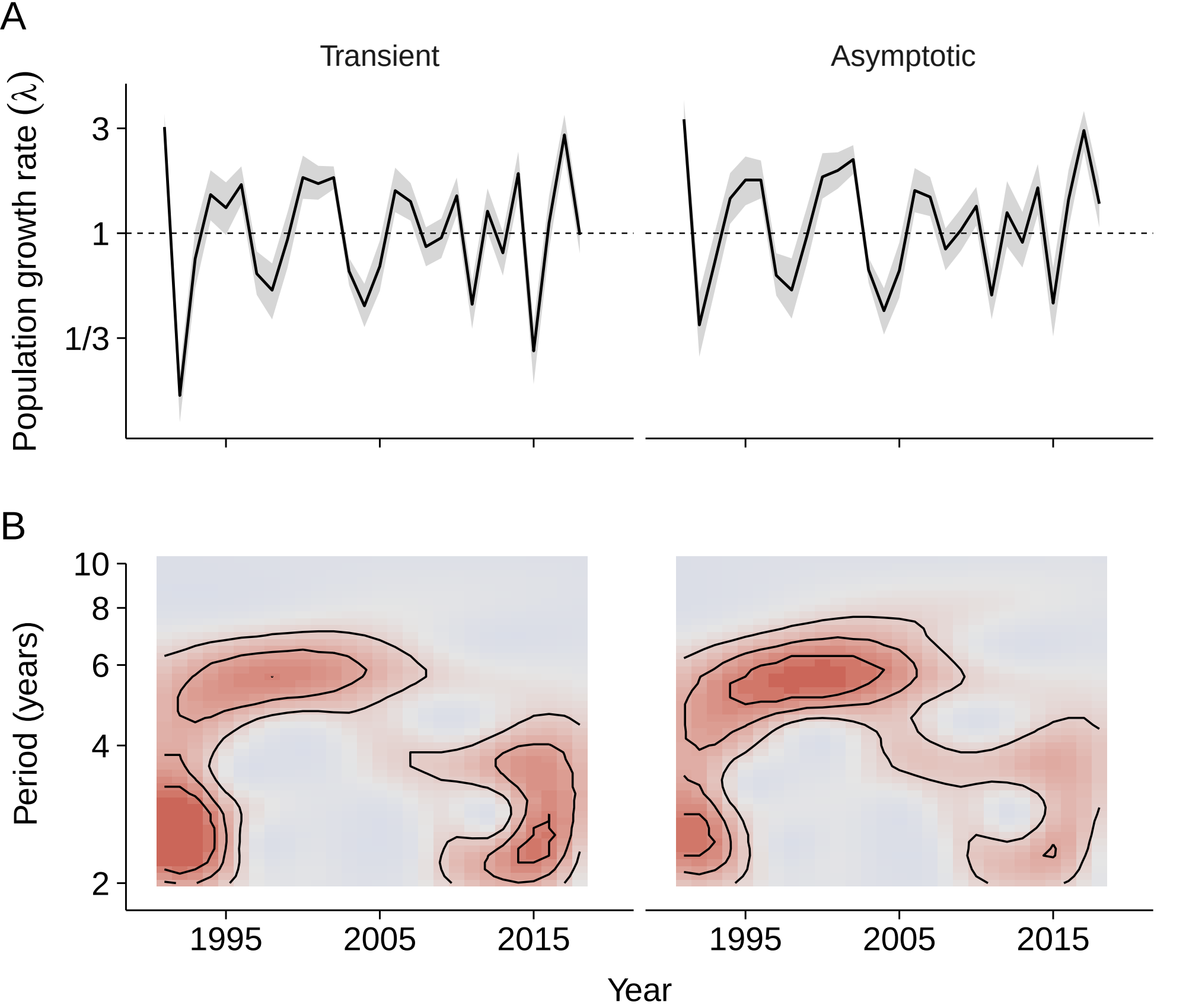
A
Transient
Asymptotic
Population growth rate (λ)
3
1
1/3
B
Period (years)
10
8
6
4
2
1995
2005
2015
1995
2005
2015
Year

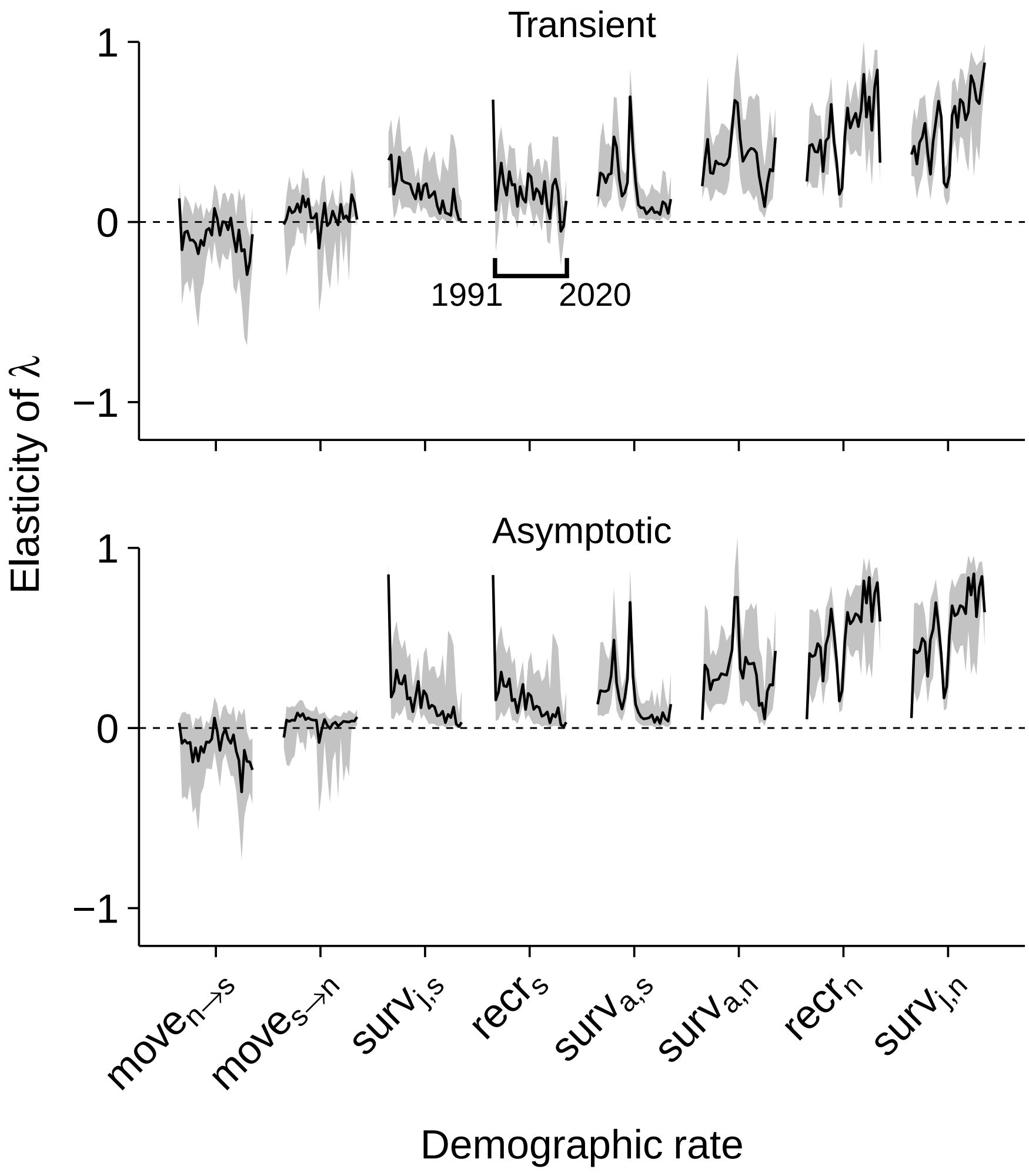
Transient
1
0
−1
1991
2020
Asymptotic
1
0
−1
Elasticity of λ
move$_{n\rightarrow s}$
move$_{s\rightarrow n}$
surv$_{j,s}$
recr$_{s}$
surv$_{a,s}$
surv$_{a,n}$
recr$_{n}$
surv$_{j,n}$
Demographic rate

Figure legends

Figure 1: (A) Distribution of trapping sites within Mývan's South (23, 27, 41, 44, and 135) and North Basins (DN, 124, and 124). Gray areas indicate water and white areas indicate land. (B) Scaled catch per unit effort (CPUE; scaled by mean) by station (thin colored lines) and posterior median scaled-CPUE from the full version of the metapopulation model (thick black lines) for each basin and stage class.

Figure 2: Scaled CPUE averaged across stations and multiplied by the relative basin area (points) with fitted values from different versions of the demographic model (lines). Solid lines are posterior medians, and shaded regions are quantile-based uncertainty intervals with coverage analogous to standard errors (68%). Note that the fitted values for the full and adult-movement models are visually indistinguishable.

Figure 3: Per capita recruitment as inferred from the adult-movement model. Solid lines are posterior medians, and shaded regions are quantile-based uncertainty intervals with coverage analogous to standard errors (68%).

Figure 4: Survival probabilities as inferred from the adult-movement model. Solid lines are posterior medians, and shaded regions are quantile-based uncertainty intervals with coverage analogous to standard errors (68%).

Figure 5: Net movement of adults between basins as inferred from the adult-movement model. We calculated net movement as the flux of individuals (in units of relative abundance) from south to north ("northward") minus the flux from north to south ("southward"). The model was formulated such that movement was calculated after survival and stage-transitions, which was reflected in the calculation of net movement. Solid lines are posterior medians, and shaded regions are quantile-based uncertainty intervals with coverage analogous to standard errors. Posterior summaries were applied to the calculation of net movement itself, rather than net movement being calculated from posterior summaries.

Figure 6: (A) Transient and asymptotic population growth rates, projected annually from the adult-movement model. Solid lines are posterior medians, and shaded regions are quantile-based uncertainty intervals with coverage analogous to standard errors (68%). The dashed horizontal line shows $\lambda = 1$, which corresponds to no change in the population size. (B) Periodograms from wavelet transforms of transient and asymptotic growth rates, with darker shading representing stronger signal associated with a given periodic element. The black contour lines are based on signal quantiles and denote regions of high signal.

Figure 7: Elasticity analysis of the transient and asymptotic population growth rates with respect to the time-varying demographic rates. Solid lines are posterior medians, and shaded regions are quantile-based uncertainty intervals with coverage analogous to standard errors (68%).

Online Supplement:

Demographic basis of spatially structured fluctuations in a threespine stickleback metapopulation,

The American Naturalist

Joseph S. Phillips[1,2,†,‡,ORCID]

Árni Einarsson[3,4]

Kasha Strickland[1,§,ORCID]

Anthony R. Ives[2,ORCID]

Bjarni K. Kristjánsson[1,ORCID]

Katja Räsänen[5,6,ORCID]

1. Department of Aquaculture and Fish Biology, Hólar University, Sauðárkrókur 551 Iceland

2. Department of Integrative Biology, University of Wisconsin-Madison, Madison, Wisconsin 53706 USA

3. Mývatn Research Station, IS-660 Mývatn, Iceland

4. Faculty of Life and Environmental Sciences, University of Iceland, 101 Reykjavík, Iceland

5. Department of Aquatic Ecology, EAWAG and Institute of Integrative Biology, ETH Zurich, Überlandstrasse 133, CH-8600 Dübendorf, Switzerland

6. Department of Biological and Environmental Sciences, University of Jyväskylä, 40014, Jyväskylä, Finland

† Present address: Department of Biology, Creighton University, Omaha, Nebraska 68178 USA

‡ E-mail: josephphillips@creighton.edu

§ Present address: School of Biological Sciences, University of Edinburgh, Edinburgh, UK EH8 9JX

Model Assessement

We fit the various model versions using Stan 2.19 (Carpenter et al., 2017) run from R 4.0.3 (R Core Team, 2020), with the `rstan` package (Stan Development Team, 2018). We used 4 chains, 20000 iterations (10000 of warm-up and 10000 of sampling), thinning interval of 2 to retain a manageable number of samples, tree depth of 11, and "adapt delta" of 0.97. Convergence was assessed by the number of divergent transitions, the potential scale reduction factor ($\hat{R}$), and the tail- and bulk-effective sample size. All of the models performed well by these diagnostics, with the exception of the "fixed rates" model, which experienced a small number of divergent transitions suggesting poor exploration of certain regions of the parameter space. This is unsurprising, as the "fixed rates" very clearly fails to characterize the data due to the large fluctuations in abundance that cannot be explained in the absence of temporally-variable demographic rates.

To complement the numerical convergence assessment, here we present some figures (S1 - S4) illustrating the successful convergence and parameter space exploration for the "adult movement" model, which was selected as the best-fitting model and served as the primary basis of our analysis.

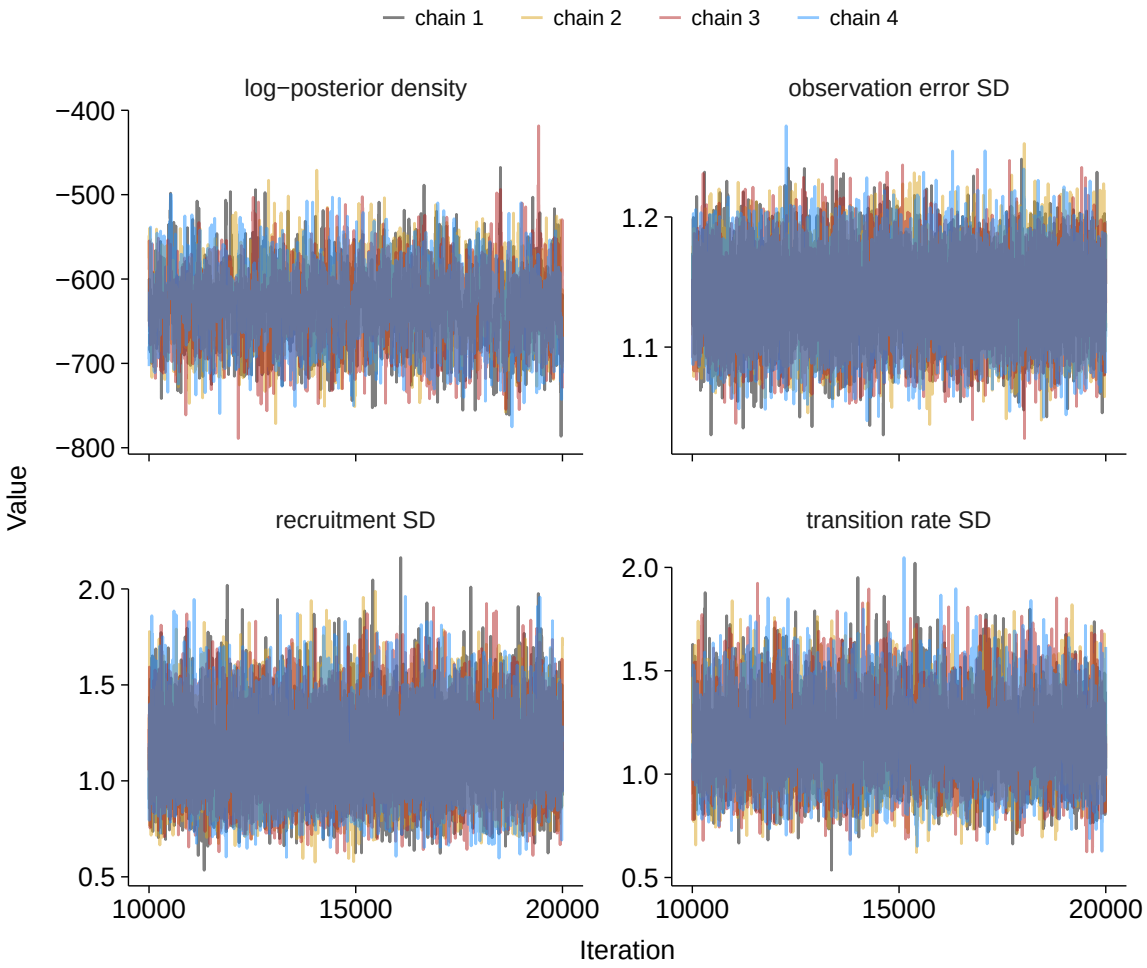

Figure S1: Trace plots showing MCMC sampling of the parameter space after the 10000 iteration adaptation phase for the "adult movement" model. Note that we used a thinning interval of 2, such that only samples from every other iteration were saved. The model has > 1500 parameters, and it would be impractical to show trace plots for them all. Therefore, we only show trace plots for several key parameters. Specifically, we show the log-posterior density, which provides a synoptic measure of the overall model fit, and standard deviations associated with observation error and temporal variation in demographic rates, which govern the basic behavior of the model in relation to the data. The trace plots indicate thorough mixing among chains, indicating effective sampling of the parameter space.

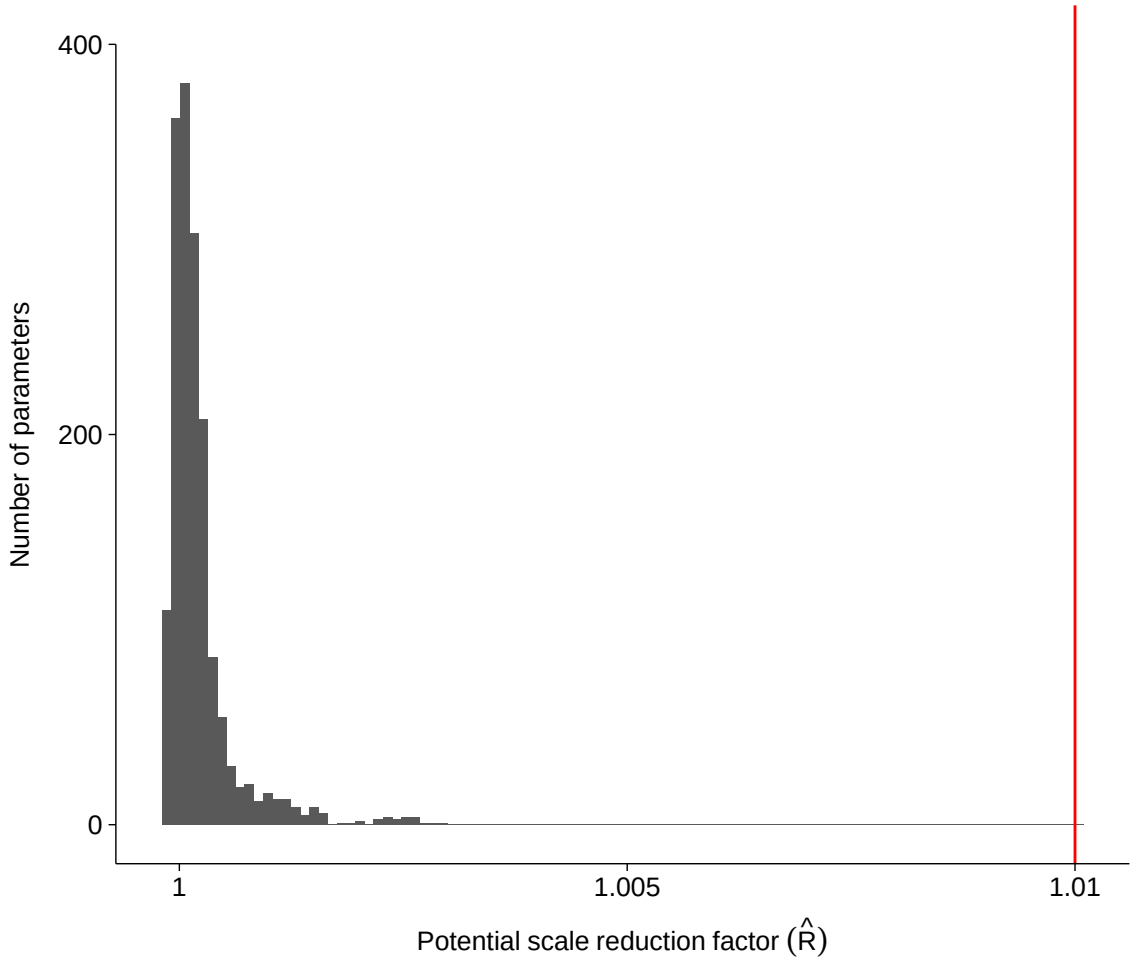

Figure S2: Histogram of potential scale reduction factors ($\hat{R}$) for all parameters of the "adult movement" model. $\hat{R}$ is a standard convergence diagnostic that approaches 1 as the sampled distribution approaches the target distribution. The vertical line denotes 1.01, which is a common threshold used to assess convergence. All $\hat{R}$'s were well below this threshold, indicating that the chains were well mixed.

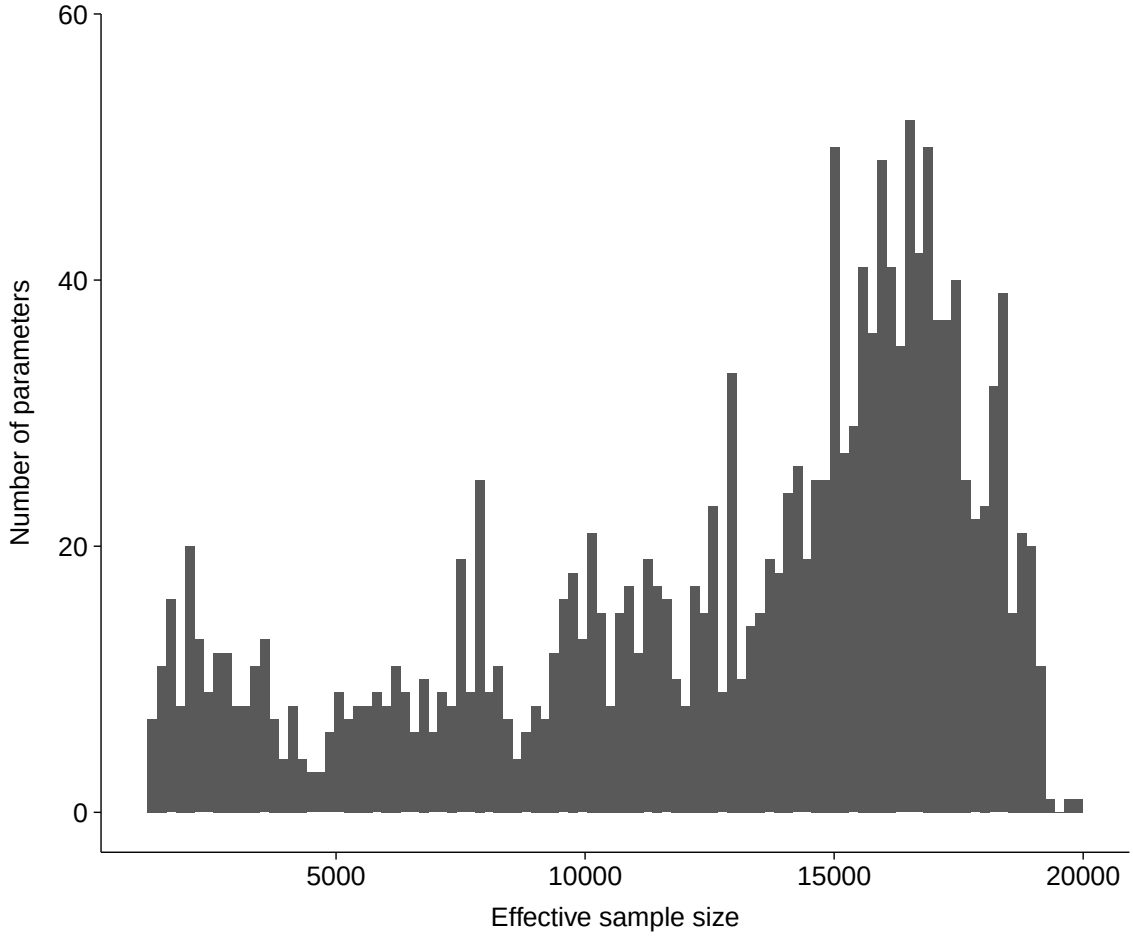

Figure S3: Histogram of effective sample sizes for all parameters of the "adult movement" model. The effective sample size is an approximate measure of the efficiency with which the parameter space is explored through MCMC. Autocorrelation in the chains reduces this efficiency, and therefore requires more iterations to fully explore the parameter space. The effective sample size was low relative to the total number of iterations for some parameters. However, lowest effective sample size of 1310 samples should provide sufficient characterization of the parameter space given that the chains were well mixed, as indicated by $\hat{R}$.

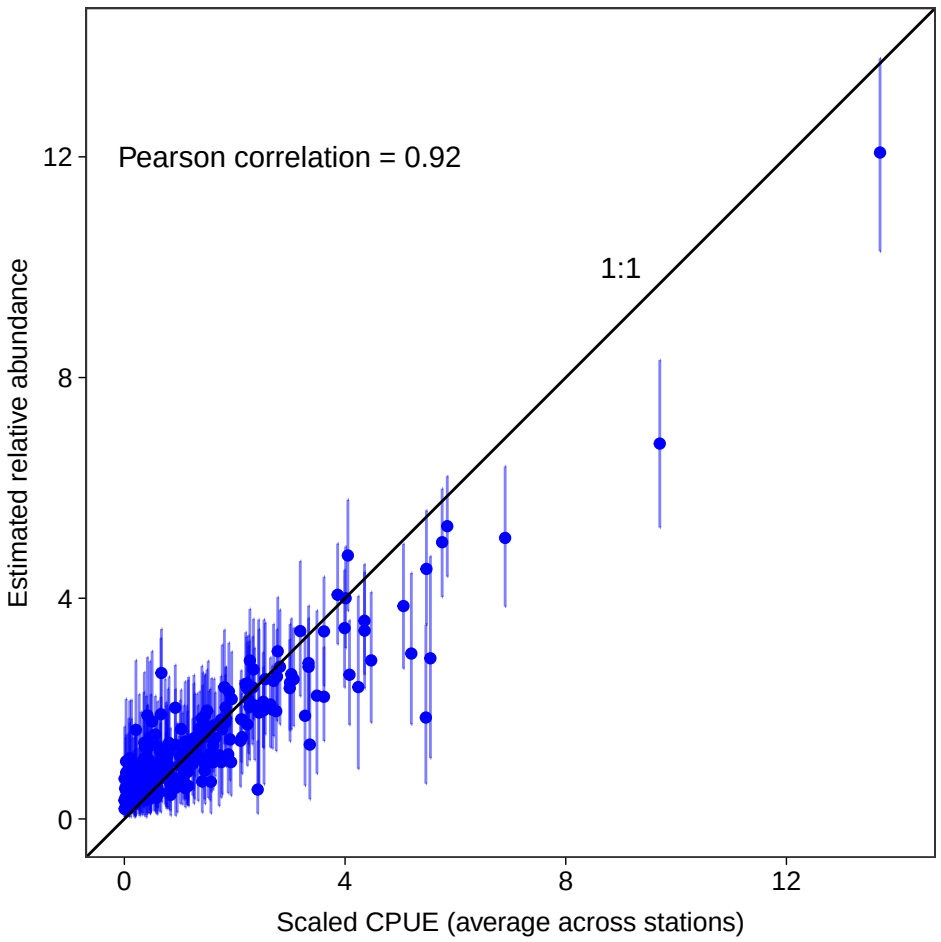

Figure S4: Estimated relative abundance for each basin × stage-class × date combination (*i.e.*, $x_{h,m,t}$) from the "adult movement" model plotted against the scaled CPUE averaged across stations and multiplied by relative basin area κ. The error bars indicate 90% posterior quantile intervals. The values deviate somewhat from the 1:1 line, with the model slightly overestimating abundance at low CPUE and underestimating at high CPUE. Nonetheless, there is a strong correlation between the observed data and the model fit.

Movement Probabilities

To characterize movement between basins, we formulated our model in terms of latent per capita movement rates ($\omega^{\delta_{h,m}}$ for stage h in basin m), from which we then calculated the probability of an individual beginning in one basin and ending in the other basin over a given time interval (main text Appendix I). While the model is parameterized in terms of separate probabilities for southward and northward movement, calculating these probabilities from latent transition rates necessarily imposes an inverse relationship between them. Moreover, because the data do not contain any information about the basin-of-origin for any given individual, only the net number of individuals exchanged between basins can be inferred as needed to account for the observed population dynamics. Therefore, in the main text we decided to present the net movement between basins. Nonetheless, for completeness we have plotted the basin-specific movement probabilities in Figure S5.

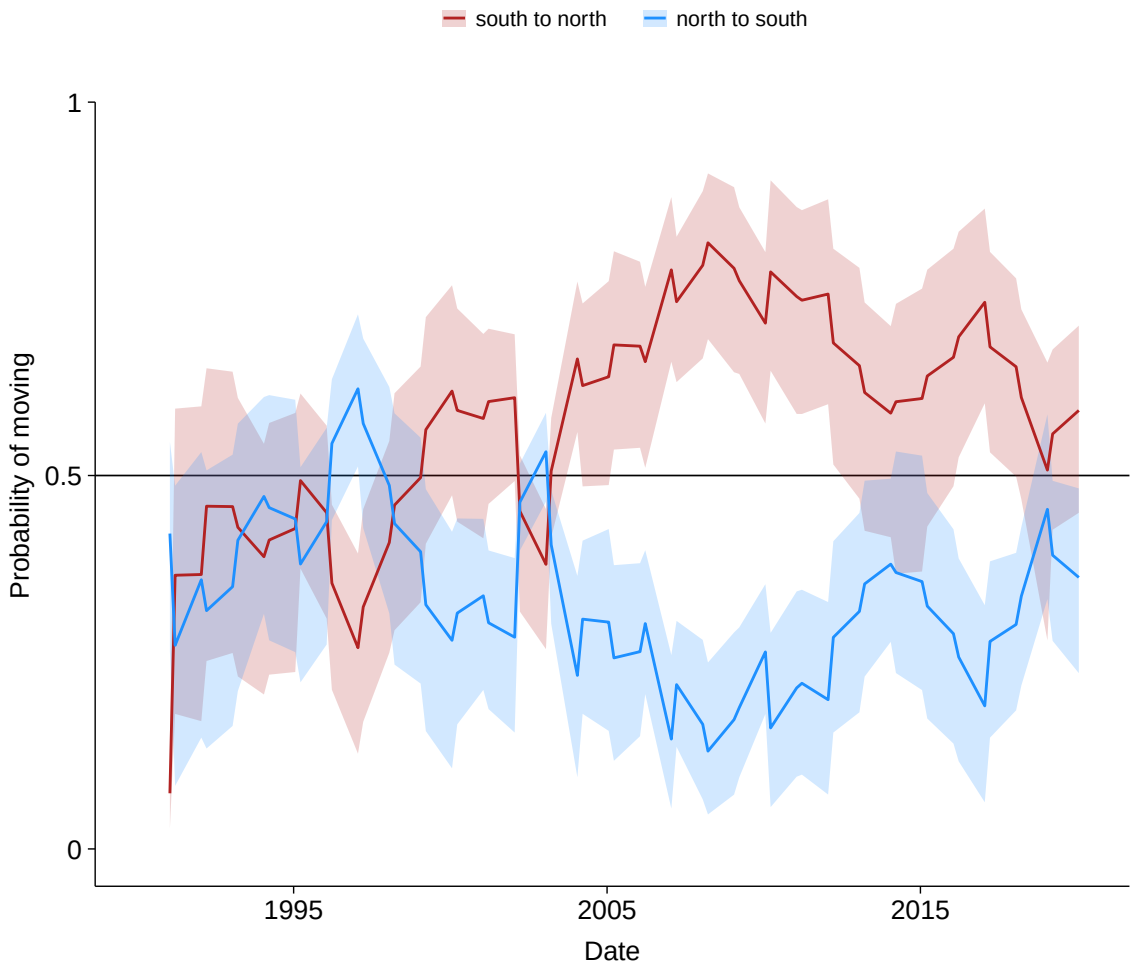

Figure S5: Basin-specific probabilities of movement between basins as inferred from the "adult movement" model. Note that while the probability of moving from south to north generally exceeds that of moving north to south, this has to be assessed in the context of the relative abundances in the two basins. Because abundance is generally higher in the north, movement from north to south generally predominates, according to the model. This underscores the relevance of considering net movement between basins (main text Figure 5) rather than the basin-specific movement probabilities.

Literature Cited

Carpenter, B., A. Gelman, M. D. Hoffman, D. Lee, B. Goodrich, M. Betancourt, M. Brubaker, J. Guo, P. Li, and A. Riddell. 2017. Stan: A probabilistic programming language. Journal of Statistical Software 76.

R Core Team. 2020. R: A Language and Environment for Statistical Computing. R Foundation for Statistical Computing, Vienna, Austria.

Stan Development Team. 2018. Rstan: the R interface to Stan. R package version 2.17.3.